Recent Advances of Hydrogel Network Models for Studies on Mechanical Behaviors

Jincheng Lei [1], Ziqian Li [1], Shuai Xu [1] and Zishun Liu [1,*]

[1]International Center for Applied Mechanics, State Key Laboratory for Strength and Vibration of Mechanical Structures, Xi'an Jiaotong University, Xi'an, 710049, People's Republic of China

*zishunliu@mail.xjtu.edu.cn

Abstract

Current constitutive theories face challenges when predicting the extremely large deformation and fracture of hydrogels, which calls for the demands to reveal the fundamental mechanism of the various mechanical behaviors of hydrogels from bottom up. Proper hydrogel network model provides a better approach to bridge the gap between the micro-structure and the macroscopic mechanical responses. This work summarizes the theoretical and numerical researches on the hydrogel network models, aiming to provide new insights into the effect of microstructure on the swelling-deswelling process, hyperelasticity, viscoelasticity and fracture of hydrogels. Hydrogel network models are divided into full-atom network models, realistic network models and abstract network models. Full-atom network models have detailed atomic structure but small size. Realistic network models with different coarse-graining degree have large model size to explain the swelling-deswelling process, hyperelasticity and viscoelasticity. Abstract network models abstract polymer chains into analytical interactions, leading to the great leap of model size. It shows advantages to reproduce the crack initiation and propagation in hydrogels by simulating chain scission. Further research directions on the network modeling are suggested. We hope this work can help integrate the merits of network modeling methods and continuum mechanics to capture the various mechanical behaviors of hydrogels.

Keywords: Hydrogel, polymer network, mechanical behavior, fracture

1. Introduction

Hydrogel is a type of synthetic polymers composed of cross-linked polymer network and water. The compliant polymer network and extremely high water content endow the hydrogel with excellent large deformation properties and biocompatibility. By modifying the polymer network, hydrogels exhibit controllable swelling-deswelling deformation under multiple external stimuli, such as temperature [1-4], humidity [5-8], light intensity [9-12], ion concentration [13-16] and magnetic field [17-19]. The excellent properties of hydrogel attract great attention from biomedicine, tissue engineering, soft machine, flexible electronic devices and other areas. At present, hydrogels have been widely used in cutting-edge research such as drug delivery [20-23], cell culture [24-27] and tissue repair [28-31] because of good biocompatibility. The excellent large deformation properties also make hydrogels a flexible substrate connecting brittle chips and circuits to human tissue to develop flexible devices [32-38]. However, for the purpose of hydrogels being a standard platform material in the human-computer interaction area, it is essential to make sure that the mechanical information of hydrogels, like deformation state, can one-to-one map to electrical signals with high precision and resolution. This requires not only advanced manufacturing techniques for hydrogels to maintain the stability of mechanical properties, but also accurate mechanics theories to describe their complex mechanical behaviors. This poses a great challenge to the mechanics researches on hydrogels.

Generally speaking, undeformed hydrogels are considered to be homogeneous and isotropic materials on macroscopic scale. Based on the homogeneous and isotropic assumption, the continuum mechanics derives the constitutive equations of hydrogels from the rigorous

mathematical description of deformation, which has been widely used to characterize the hyperelastic, viscoelastic and poroelastic large deformation of hydrogels [39-42]. These constitutive equations usually involve a series of material constants [43-48] which can be determined from elaborate standard mechanical tests. Then, the constitutive equations can be numerically implemented to simulate arbitrarily complex structures under different boundary conditions [43, 49]. However, the constitutive equations are often unable to simultaneously capture the stress-strain relationships under multiple loading conditions, and their accuracy is challenged under large deformation especially near fracture. It inspires us to investigate the fundamental mechanism of multiple mechanical behaviors from the underneath microstructure of hydrogels. Obviously, the homogeneous and isotropic assumption ignores the randomness of the hydrogel network structure. Constitutive equations attempt to use few material constants to capture the complex deformation of random polymer network, which make it hard to describe extremely large deformation and fracture. One example is that fracture criterion or damage factor is often needed as extra constraints on constitutive equations to characterize failure [50-55]. Fracture criterion gives an exact critical value to generate crack. Crack breaks the continuity of material, which makes it hard to be implemented in FEM simulations. So far, the crack propagation, bifurcation and intersection have not been well realized in FEM simulations. Damage mechanics alleviates this deficiency of the fracture criterion. By introducing a damage factor related to the deformation state, the mechanical properties are gradually weakened in a continuous manner during deformation [56]. For example, damage mechanics has been applied to simulate the crack growth in hydrogel implemented in phase field method [57-59]. Similar to the constitutive equations, parameters in fracture criterion and the relationship between deformation and damage factor in damage mechanics also need to be obtained from experiments

or just hypothesis. Besides the mechanics framework, machine learning is able to directly train a load-deformation relationship accurately[60]. Nevertheless, it requires massive high quality experimental data, and the trained coefficients have no physical meaning actually. In short, continuum mechanics and machine learning cannot reveal the deformation and failure mechanism of hydrogel materials from bottom up, and thus cannot guide the hydrogel reinforcement and multi-functionality [61].

In fact, researchers have realized the importance of the microstructure of hydrogels. Since water in hydrogels has quite limited influence on its mechanical properties, most of the research works focus on the mechanical properties of the polymer network. The most fundamental models of hydrogel polymer network can be constructed using full-atom molecular dynamics (MD) [62-67]. The deformation and breaking of covalent bonds are both intrinsically incorporated in the widely-accepted interatomic potentials in full-atom MD, so that the conformation change and the fracture of polymer chains can be clearly displayed in microscopic level. However, due to the limitation of computing power, these full-atom models are so small and usually only contain several cross-linked polymer chains. Despite fully capture the atomic details, they cannot reflect the overall randomness of the real hydrogel network [67-69]. In order to break through the limitations of computing resources to simulate larger models, coarse-graining (CG) method is adopted by discarding atomic details in exchange for larger model size [70-74]. Using CG method, hydrogel network models with much more polymer chains can be constructed by directly mimicking the real crosslinking process. These models can already show the real features of hydrogel network, such as branch chains, isolated chains, entanglement, etc. [73, 74] The prominent advantage of hydrogel CG models is that it vividly reveals the underlying mechanism of the viscoelasticity and fracture, but the quantitative mechanical properties often

cannot match the experiments well. There is still a gap between CG models and the continuum hydrogel. Therefore, a deeper understanding on the structure of hydrogels from bottom up is still in urgent need.

As a typical synthetic polymer, the internal structure of hydrogel network exhibits distinct structural features and mechanical properties on several length scales as shown in Fig. 1. (i) Persistent length: The persistent length is a length of Kuhn segment [75] which can be regarded as a rigid segment in a polymer chain. The Kuhn segment in synthetic hydrogel polymer chain is generally composed of several interconnected monomer molecules with length scale ~1 nm. Its mechanical properties are dominated by the energy of covalent bonds inside. (ii) Chain length: A polymer chain in hydrogel is generally formed by dozens or hundreds of connected rigid segments, with the contour length scale ~100 nm and end-to-end distance ~10 nm. Because of the effect of intermolecular forces and thermal fluctuations, chains generally curl up and are quite soft. Their mechanical properties are dominated by the change of conformational entropy. (iii) Network scale: Hydrogel network is composed of cross-linked polymer chains whose length distribution is quite random. The mechanical properties of the network are not only dominated by the conformational entropy of all chains, but also affected by the interaction between adjacent chains, as well as between chain and water.

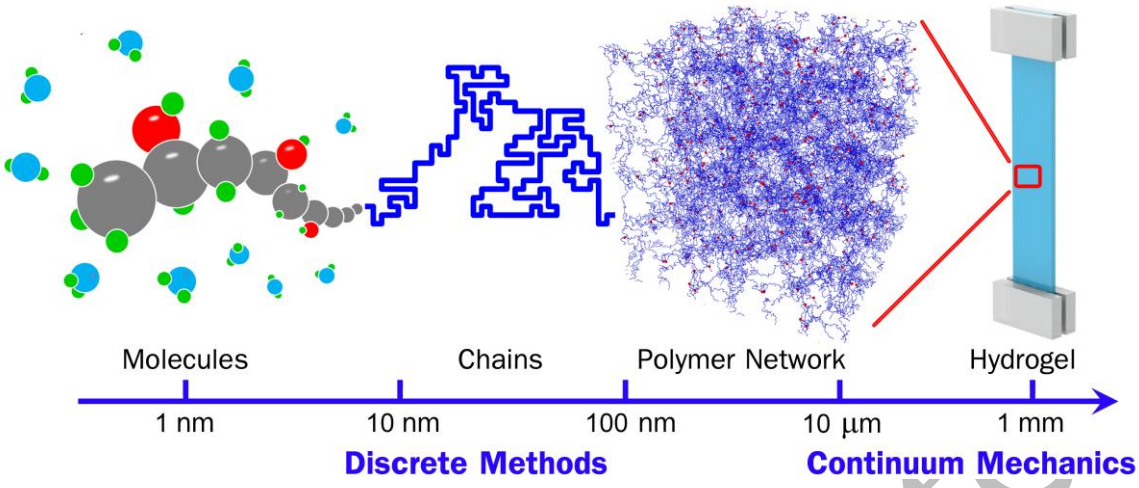

Figure 1 The length scales in hydrogel.

For molecules, polymer chains and network, discrete modeling methods are adopted to characterize their mechanical behaviors because of the significant randomness caused by heat fluctuations. On contrast, continuum mechanics overlooks the intrinsic discontinuity. Hydrogel polymer network can act as a bridge connecting the microscopic nature and the macroscopic mechanical responses. Thus, proper hydrogel network models are in urgent need to essentially describe multiple mechanical behaviors of hydrogels. Current researches on the hydrogel network models are scattered and fragmented. This article systematically summarizes the current theories and numerical simulations on hydrogel network models, and provides a discrete perspective to investigate the macroscopic mechanical behaviors.

This article is organized as follows. Section 2 introduces current construction and analysis methods of hydrogel network models. Section 3 summarizes the applications of different types of hydrogel network models on multiple mechanical behaviors, including swelling behavior, hyperelasticity, viscoelasticity and fracture. Section 4 discusses the

advantages and disadvantages of current hydrogel network models, and proposes new research directions for the network modeling methods. Concluding remarks are given in Section 5.

2. Hydrogel Network Model

Continuum mechanics refines the mechanical response of materials into phenomenological theories, and then applies the theories to complex cases. Unlike continuum mechanics, discrete modeling method constructs particle-based structural models, applies the fundamental laws, such as Newtonian mechanics, to directly simulate the bulk mechanical response. However, it often requires proper simplification on models to reduce computational costs. Thus, the validity of models is often the major concern about discrete modeling method.

Building a hydrogel polymer network model is the first step to study the mechanical properties of hydrogels from a discrete perspective. Basically, we can divide the existing hydrogel network models into three categories, namely the full-atom network models, realistic network models and abstract network models. Figure 2 shows the three categories of network models and the corresponding modeling methods. Full-atom network models provide all the atomic details of the polymer network, such as chemical bonds, bond angles and dihedrals etc. They are often constructed and simulated by MD. Realistic network models simplify the atomic details of full-atom network models by a coarse-graining process, leading to larger model size. Coarse-grain molecular dynamics (CGMD) and dissipative particle dynamics (DPD) are widely used in constructing and analyzing realistic network models. MD, CGMD, and DPD belong to microscale models because the characteristic lengths of their structural models are still in the microscale. The self-avoiding walking (SAW) method generates realistic network models with detailed chain configurations, while the user-defined coarse-graining degree makes these models

can be microscale models or mesoscale models. Abstract network models replace the concrete chain configurations with simple interactions with respect to the chain end-to-end length. Ideal network models and stochastic topological network (STN) models are two typical types of abstract network models. They belong to mesoscale models because the characteristic lengths of these models, i.e. the chain length, are in mesoscale. In this section, we introduce the construction and simulation details of these three categories of hydrogel network models.

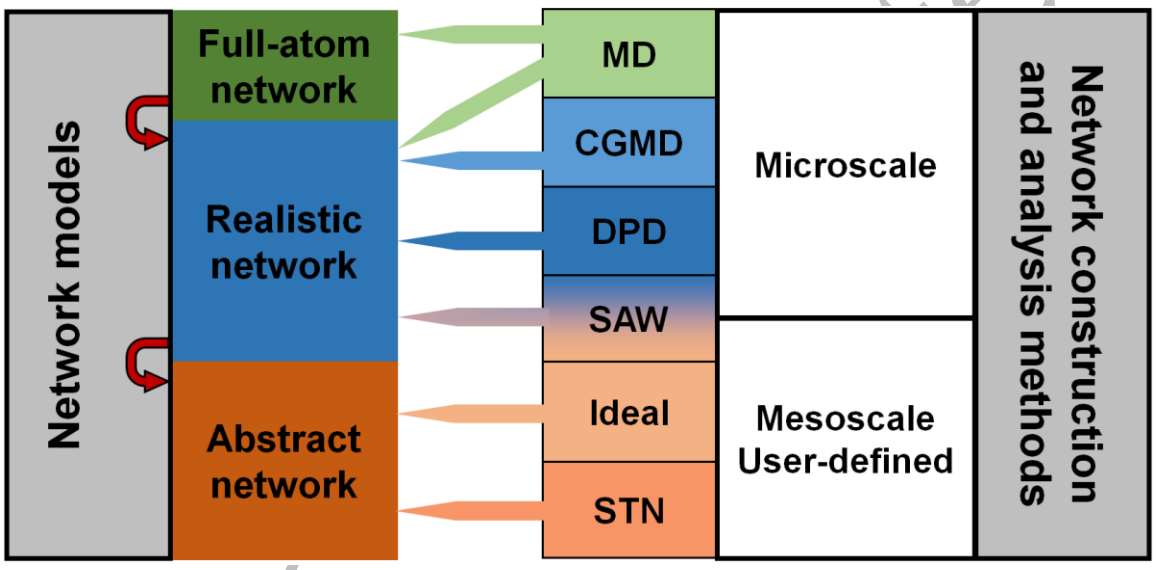

Figure 2 Three categories of hydrogel network models with their construction and simulation methods. The left part lists three categories of network models: full-atom network model, realistic network model and abstraction network model. Red arrows indicate the increasing of the coarse-grainning degree in three categories of models. The right part lists commonly used construction and analysis methods.

2.1 Full-atom network model

The most fundamental realistic network models of hydrogels are constructed by the full-atom MD method. The full-atom MD uses force field to define the interatomic interaction of

various atoms, including van der Waals interactions, electrostatic forces, chemical bonds, bond angles, dihedrals and impropers. Many reliable force fields have been developed for polymer system, such as the consistent valence force field (CVFF) [76] , optimized potentials for liquid simulations (OPLS) force field [77], GROMACS force field [78] and DREIDING force field [79] etc. The motion of the atoms is governed by Newtonian mechanics as follows

$$\boldsymbol{F} = -\frac{\partial V}{\partial \boldsymbol{x}}, \boldsymbol{F} = m\ddot{\boldsymbol{x}} \tag{1}$$

where $\boldsymbol{F}$ is the force on each atom with the coordinate $\boldsymbol{x}$, V is the interactive potential energy of the system calculated by interactive force field, m is the atomic mass.

A full-atom hydrogel network model is generally constructed with the following three procedures. (i) The atomic structures of monomers, crosslinkers and water molecules are constructed as the basic components. (ii) Arrange the location of monomers, crosslinkers and water molecules, create bonds and form a polymer network structure. (iii) An additional relaxation simulation is performed to optimize the hydrogel network model in a desired density. The most important part is the second procedure. Many crosslinking strategies are proposed to accomplish the network model construction. In Deshmukh's work [63], the polymer chain between two crosslinkers with pre-fixed locations is gradually grown using a self-avoiding walk algorithm. A cutoff parameter is adopted to control the length distribution of generated polymer chains. Water molecules are added in remaining vacant spot. In Ou et al.'s [65] work and Jiang et al.'s [66] work, monomers and crosslinkers were randomly mixed as solution, and then directly crosslinked into polymer network. Water molecules were added after generating the polymer network. However, limited by computing power, a full-atom hydrogel network model often contains only several polymer chains as the periodic representative volume element of hydrogel

network, instead of showing the full picture of the hydrogel polymer network. Hence, this type of models [80] is usually arranged in a periodic simple-cubic lattice. Other types of lattice arrangement of hydrogel models [63, 69, 80] can also be realized by tuning the coordination number of crosslinkers, such as the diamond lattice arrangement [63] and body-centered lattice arrangement [69].

We constructed full-atom models of polyacrylamide (PAAm) hydrogel [62, 81] using two methods. The first method is to form a hydrogel network with the lattice arrangement of polymer chains. In this hydrogel network model, each polymer chain has 50 repeat units of acrylamide molecules. 2,4,6-trimethylolphenol was chosen as the chemical crosslinker to provides 6 crosslinking sites for the polymer chains to be arranged in simple-cubic lattice. Figure 3 shows a 2*2*2 periodic hydrogel network model. The lattice type of models usually have neat polymer network without side chains. In order to mimic the real polymer network, we also constructed a PAAm hydrogel model by simulating the crosslinking process of acrylamide (AAm) and N,N'-methylenediacrylamide (MBAA) molecules. 333 acrylamide molecules and 22 MBAA molecules were packed into a block region as shown in Fig. 4(a). A crosslinking simulation was performed to form C-C bonds between crosslinking sites when the distance is below 5 Å. Water molecules were then inserted into the crosslinked hydrogel network, following with a relaxation simulation for structural optimization. As shown in Fig. 4(b), the constructed PAAm hydrogel models show the realistic structural features, including the crosslinked network, branch chains and unreacted units. These full-atom hydrogel network models are usually used to investigate the microscopic properties, such as hydrogen bond distribution, water absorption and thermal conductivity. It is still too small to reflect the mechanical properties in a statistical manner.

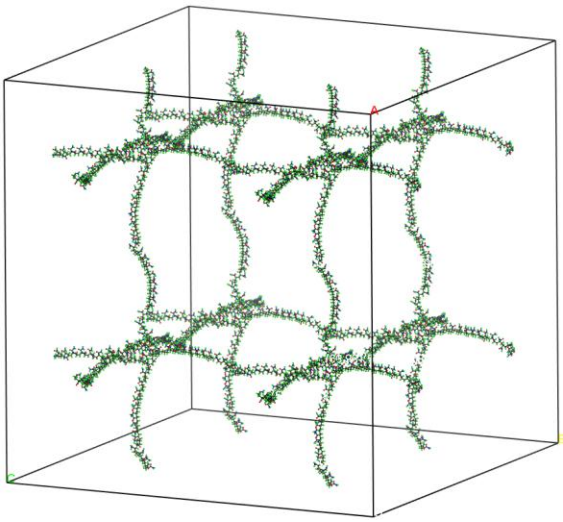

Figure 3 A PAAm hydrogel network model with the simple-cubic arrangement of polymer chains[62]

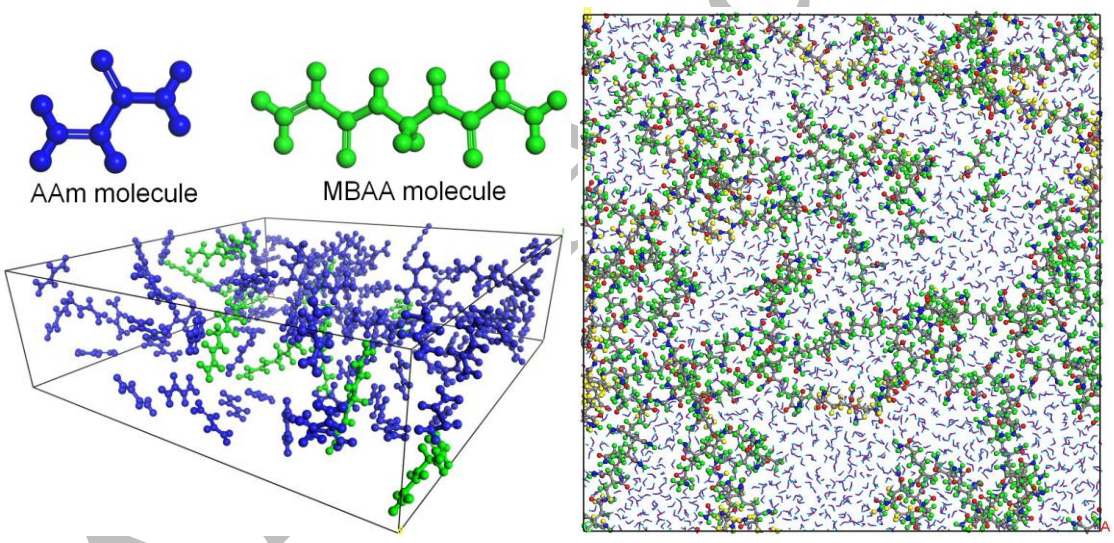

(a) (b)

Figure 4 The PAAm hydrogel network model[81] constructed by simulating the crosslinking reaction. (a) Initial configurations of the reaction system with AAm and MBAA molecules. (b) The constructed hydrogel network model.

2.2 Realistic network models

Coarse-grain molecular dynamics (CGMD) is an effective method to increase the scale of the microscopic model of hydrogel. It follows the dynamics framework of full-atom MD in Equation (1). By integrating multiple atoms into a single particle in structure and interaction force field, coarse-graining (CG) method achieves larger model size and time scale. For instance, the MARTINI CG method [82] is a well-established CG method for lipid system, including the mapping scheme from certain atomic groups to CG particles and the well-trained force field for CG particles. Several heavier atoms, such as C, N and O atoms, together with the attached H atoms are mapped into one particle. Through structural mapping, the four-body dihedral and improper interactions in full-atom MD are eliminated. Zhang et al. [70] and Salahshoor et al. [71] constructed hydrogel network models using MARTINI CG method to investigate the transport properties in micro-scale. In fact, there is no generic method for CGMD simulations. Researchers have to determine the CG degree with the balance of the interested properties and the computational resources, and then conduct parameter training of CG force field. In order to simulate the solution system, the dissipative particle dynamics (DPD), or Brownian dynamics, allows several water molecules to be mapped into one particle. DPD introduces the friction force between CG particles and random force caused by the collision of adjacent CG particles to characterize the heat fluctuations in larger length scale and time scale

$$\boldsymbol{F}^C + \boldsymbol{F}^D + \boldsymbol{F}^R = m\ddot{\boldsymbol{x}} \tag{2}$$

where $\boldsymbol{F}^C$ is the conservative force between two particles, $\boldsymbol{F}^D$ is the dissipative force (or friction force), $\boldsymbol{F}^R$ is the random force. The conservative force adopted in DPD is a soft repulsive force linearly decaying to zero with respect to distance between particles. The dissipative force and random force correspond to the energy dissipation and source, respectively, keeping the

thermodynamic equilibrium of the simulation system. DPD reduces the atomic heat fluctuations into slower heat fluctuations in larger length scale, which increases the time scale of the simulation system at the same time.

Bead-spring model is the most widely used CG model to simulate hydrogel system. A polymer chain is usually mapped into a string of beads, where beads represent one or more monomer molecules. The harmonic bond with the potential function $V = K\left(r - r_0\right)^2$ is frequently used, where *K* is the bond energy coefficient, r is the bond length between beads, the equilibrium length r0 is usually taken to be 0, i.e. pure attractive, in many DPD simulations [73, 83-86]. The finite extensible nonlinear elastic (FENE) potential [72, 87-89] with $V = -0.5KR_0^2 \ln\left[1-\left(r / R_0\right)^2\right]$ also defines a bead interaction with the maximum bead distance R_0. Except the specific atomic configurations, the construction procedure of bead-spring models is similar to that of full-atom models. One method is to directly arrange beads and chains into lattice network structure. For instance, Chen et al. [72] used DPD to build a hypothetical tetra-functional hydrogel network model with the diamond-lattice arrangement of straight polymer chains. Chains with curly conformation are more common to be arranged into diamond lattice to form hydrogel network models [90-94]. Another method is to simulate the crosslinking reaction between beads to create hydrogel network models. Wei et al. [73] generated the random hydrogel network model of polyvinyl alcohol/polyacrylamide hydrogel by simulating the crosslinking of monomer beads and crosslinker beads, then inserted water molecules later into the vacant spot.

Crosslinking reactions don't always generate polymer network. In order to reproduce the crosslinking process of PAAm hydrogel, we used DPD to simulate the crosslinking reactions of PAAm solution with AAm beads, MBAA beads and water beads [74]. As shown in Fig. 5(a),

one CG bead in our simulations represents two AAm molecules, or eight water molecules, or one MBAA molecules. Simulations show that sufficient mean square displacement (MSD) of beads and proper water content are two crucial factors to form hydrogel network. When MSD of beads per simulation time unit is below the mean distance of beads, it leads to local crosslinking and forms small polymer loops. On the contrary, when MSD is far larger than the mean distance of beads, it forms global polymer network as shown in Fig. 5(b). It also predicts the water content 97% is the upper limit to form a hydrogel network, which is quite close to the swelling limit of PAAm hydrogel. Above simulations not only reveal the crosslinking mechanism of PAAm hydrogel, but also construct hydrogel network model with realistic structural features, such as the branch chains (grey chains in Fig. 5(b)), isolated chains (yellow chains in Fig. 5(b)) and loops (magenta chains in Fig. 5(b)).

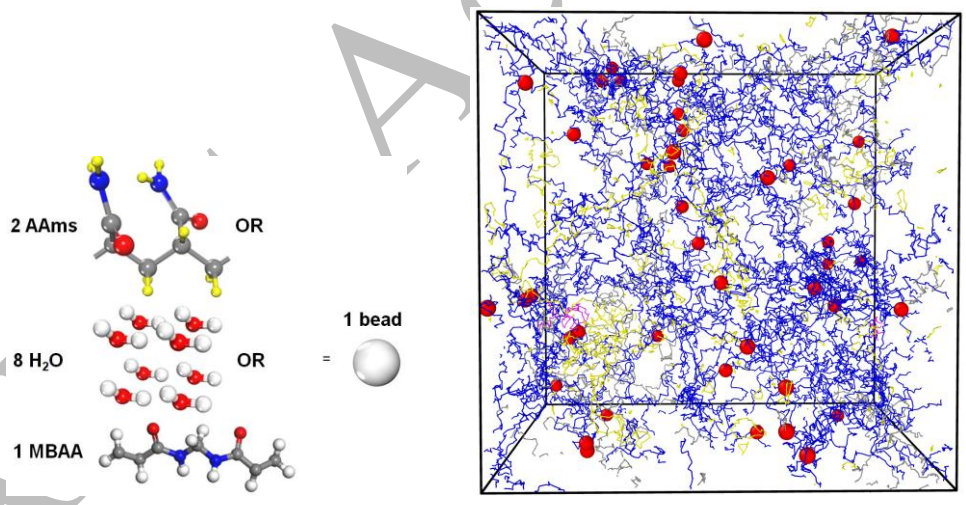

(a) (b)

Figure 5 A realistic network model of PAAm hydrogel and the corresponding CG mapping method [74]. (a) One CG particle represents two AAm molecules, or eight water molecules, or one MBAA molecules. (b) Bead-spring models of PAAm hydrogel without displaying water

particles. Blue strings are polymer chains forming network. Grey strings are branch chains attached on network. Yellow strings are isolated chains. Magenta strings are the isolated loops. Red beads are crosslinker beads.

Besides the particle-based dynamics description of polymer network, we also adopted self-avoiding walking (SAW) algorithm to reproduce the complex conformation of the hydrogel polymer network. A SAW trajectory is a sequence of distinct points that does not superpose in an arbitrary dimensional lattice. As shown in Fig. 6(a), we developed a SAW algorithm and generated a series of SAW trajectories to represent polymer chains. [95, 96] Despite these trajectories are limited in square 2-D lattice and simple-cubic 3-D lattice, they reflect the curl and fractal properties of long polymer chains with considering self-repulsion. This SAW algorithm was further upgraded to generate periodic hydrogel network models by introducing the split of the walking trajectory as shown in Fig. 6(b). By controlling the split probability in each step, polymer network with random chain lengths can be generated as shown in Fig. 6(c). This modeling method can be further improved by replacing each trajectory nodes with monomer (or crosslinker) molecules or CG particles to generate particle-based models.

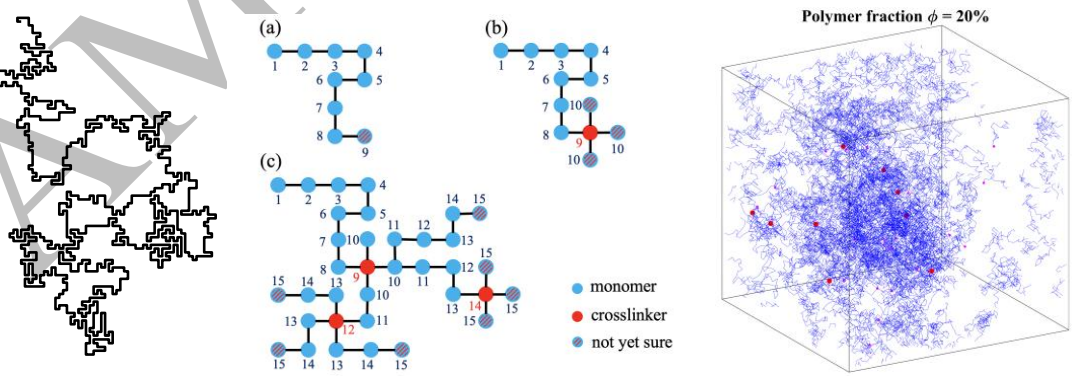

(a) (b) (c)

Figure 6 Construct network model using SAW algorithm [95]. (a) A 2-D SAW trajectory represent a polymer chain. (b) Schematics of generating the network model. The red dots represent the crosslinkers. SAW trajectory splits from each crosslinker into three branches. (c) A 3-D polymer network model with the polymer fraction 20%.

2.3 Abstract network model

Generally, hydrogels with high water content have long and soft polymer chains relying on the short persistent length. The persistent length of hydrogel polymer chains is generally considered less than 1 nm, while the contour length of polymer chains in hydrogels is generally far greater than 1 nm. This indicates that the bending stiffness of polymer chains in hydrogels can be ignored. Therefore, the free energy of a hydrogel polymer chain is considered to be only determined by the conformation entropy related to the end-to-end distance. For example, a quadratic configurational entropy $W_{Gaussian}$ is derived based on the Gaussian chain hypothesis [97]

$$W_{Gaussian} = \frac{3kT}{2}\left(\frac{r}{r_0} - 1\right)^2 \tag{3}$$

where kT is the energy unit in thermodynamics, r is the chain end-to-end distance, r_0 is the initial end-to-end distance. When a curly polymer chain is stretched to straight, its free energy transitions from entropy-dominated to bond energy-dominated, corresponding to the dramatically increase of the tensile force. In order to describe this so-called non-extensibility, Langevin-type chain model [75] and worm-like chain (WLC) model [98] are proposed as the following force-elongation relation

$$F_{Langevin} = \frac{kT}{b} L^{-1}\left(\frac{r}{nb}\right)$$
$$F_{WLC} = \frac{kT}{b}\left\{\frac{r}{nb} + \frac{1}{4\left[1-r/(nb)\right]^2} - \frac{1}{4}\right\} \quad (4)$$

where L^{-1} is the inverse Langevin function with $L(x) = \coth(x) - 1/x$, nb is the chain contour length with the length of Kuhn segment b and number of Kuhn segment n. Further, polymer chains are considered to be constrained in a tube-like region by adjacent polymer chains [99-101]. A tube model [101] considering the constraint effect is proposed with the free energy form

$$W_{tube} = \alpha kT\left(\frac{r_0}{d}\right)^2 \quad (5)$$

where α is a shape factor of the cross section of polymer chain, d is the effective diameter of the tube region. Above four chain models have been used to quantitatively describe the tension-contraction response of polymer chains. It facilitates researchers to neglect the concrete chain conformation and replace it with simple analytical interactions instead. Hydrogel network models constructed in this way are abstract network models. Abstract network models can be regarded as the CG model of realistic network models. It not only shows the bulk mechanical behaviors of the entire polymer network, but also captures the tension-contraction behavior of every polymer chain. Here we introduce several typical abstract network models.

Ideal network model is the simplest abstract network model. It assumes that all polymer chains in network have equal contour length and end-to-end distance. Figure 7 shows two types of ideal network models. Ideal network assumption is the basic assumption for many constitutive theories in continuum mechanics because of the following two merits. First, the summation of the free energy of all chains can be simplified as a concise analytical form. One example is the

Neo-Hookean constitutive model $W = \frac{nkT}{2}(I_1 - 3)$. Based on the assumption of equal chain length and the uniformly distributed orientation of polymer chains, the Neo-Hookean model integrates the complex deformation of all chains as a simple scalar, i.e. the first invariant I_1 of the bulk deformation gradient. Second, the ideal network assumption implies the affine deformation of the entire ideal network, which exactly conforms to the basic assumption of continuum mechanics. For instance, Arruda et al. [102] proposed an ideal eight-chain network model (Fig. 7(b)) with the assumption of affine deformation, and also linked the individual chain stretch to I_1 with

$$\lambda_{chain} = \sqrt{\left(\lambda_1^2 + \lambda_2^2 + \lambda_3^2\right)/3} = \sqrt{I_1/3} \tag{6}$$

The well-known Arruda-Boyce model has been successfully applied to characterize the hyperelasticity of rubber. One step further, it is reasonable to consider that all constitutive theories with respect to I_1 imply the ideal network assumption. We also proposed a series of constitutive models of hydrogels based on ideal network assumption. Some other researchers used tube model to consider the non-affine deformation of polymer network and proposed so-called non-affine constitutive models [100, 101]. However, these models still hold the ideal network assumption when integrating all the chain stretch [103].

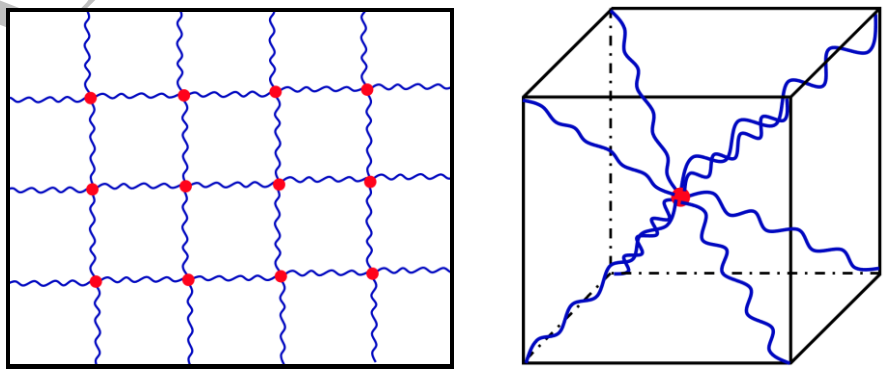

(a) (b)

Figure 7 Two types of ideal network model. (a) A 2-D square ideal network model. (b) A 3-D eight-chain ideal network model.

Real hydrogel polymer network is far more complicated than ideal network models. The current gelation techniques of hydrogels determine the random polymer network with a large number of entanglements and the wide distribution of chain contour length and end-to-end distance. Consequently, the assumption of affine deformation also fails [104, 105]. In order to consider the structural randomness and the non-affine deformation of hydrogel network model, abstract network models with random chain length are constructed. These models are composed of crosslinkers with random locations and their connections representing polymer chains. We name these models as stochastic topological network (STN) models and give the governing equations of deformation. The total free energy W of a STN model is the summation of the free energy of every chains with respect to the location of all crosslinkers $\boldsymbol{x}$

$$W(\boldsymbol{x}) = \sum_i W_i \tag{7}$$

Then, the governing equation of the dynamics of the STN model can be generalized as

$$\boldsymbol{F}_j = -\frac{\partial W}{\partial \boldsymbol{x}_j}, \boldsymbol{F}_j + c\dot{\boldsymbol{x}}_j + m_j\ddot{\boldsymbol{x}}_j = 0 \tag{8}$$

where $\boldsymbol{F}_j$ is the resultant force on crosslinker j, c is the damping coefficient, m_j is the effective mass of crosslinker j. The deformation of STN model can be realized by developing algorithms to solve Equation (9) [106, 107] under boundary conditions. Alame et al. [108] built 2-D STN models to investigate the elasticity of the tetra-arm PEG hydrogels. They adopted the Langevin chain model and investigated the coordination number effect of crosslinkers. Kothari et al. [109]

also built a 2-D STN models using the WLC model to investigate the fracture behaviors of hydrogel network. The numerical implementation of STN model is quite similar to finite element method, since both methods lead to the equation set of $\boldsymbol{K} \cdot \boldsymbol{x} = \boldsymbol{F}$, where $\boldsymbol{K}$ is the stiffness matrix, $\boldsymbol{x}$ is the coordinate vector of all nodes and $\boldsymbol{F}$ is the force vector on all nodes. This similarity makes it possible to unite the simulations of continuum elements and STN models, as long as the free energy forms in continuum mechanics and STN models are compatible.

3. Mechanical Behaviors of Hydrogel

In this section, we show some applications of network models on the mechanical problems of hydrogels, including swelling behavior, hyperelasticity, viscoelasticity and fracture. For swelling properties, network models are able to (i) determine the upper limit of water content and (ii) calculate the effect of water content on the elastic modulus of hydrogels. For hyperelasticity of hydrogels, network models can (i) directly calculate the stress-strain curve without constitutive equations, and (ii) demonstrate the rationality of ideal network assumption within finite deformation. For viscoelasticity of hydrogels, network models reveal two origins of viscoelasticity. One is caused by the accumulated fracture of chains and the other one comes from the friction between chains. For fracture behaviors of hydrogels, network models can (i) calculate the evolution process from initial deformation to total fracture and (ii) monitor the fractured state of each chain within a network. Figure 8 lists the applicability of three categories of network models on the mechanical behaviors of hydrogels.

Mechanical behavior / Models	Swelling	Hyperelasticity	Viscoelasticity	Fractrue
Full-atom network	✓			✓
Realistic network	✓	✓	✓	✓
Abstract network	✓	✓	✓	✓

Figure 8 The application of three categories of network models on the mechanical behaviors of hydrogels. All network models can be used in the investigation of swelling and fracture behaviors. Hyperelasticity and viscoelasticity commonly require larger-scale network models, i.e. realistic network and abstract network.

3.1 Swelling-deswelling behaviors

The hydrophilic polymer chains in hydrogels can absorb large amount of water molecules, leading to the extremely high water content of hydrogels. It is thought that the main driving force of hydrogel swelling is the energy reduction caused by hydrogen bonds between chains and water. The swelling process to equilibrium can be considered to reach a compromise between hydrogen bond formation and chains stretching. From a continuum mechanics perspective, when a hydrogel reaches the swelling equilibrium, it can establish an equilibrium equation between internal and external chemical potential $\mu_{in} = \mu_{ext}$. The problem is that chemical potential cannot be measured in experiments. Current constitutive theories suggest chemical potential value can be obtained by free boundary conditions as follows

$$\frac{\partial W\left(\boldsymbol{F}_s,\mu\right)}{\partial \boldsymbol{F}_s}=\mathbf{0} \tag{9}$$

where W is the free energy of hydrogels with respect to the swelling deformation gradient $\boldsymbol{F}_s$ and chemical potential μ. Above equation subtly determines the chemical potential as the stretching force of hydrogel network during swelling. However, this doesn't provide any insight on the microscopic nature of chemical potential. On contrast, the swelling theories established from a microscopic view reveal the mechanism of swelling. Katchalsky's work [110] on the swelling of polyelectrolyte gels laid the foundation of the microscopic theory of swelling. Katchalsky et al. thought that the swelling equilibrium of hydrogels is determined by the balance between the internal stress of polymer chains and the osmotic pressure on chains from solvent environment, i.e. $P_{in}=P_{ext}$. The internal stress of polymer chains can be obtained as the differential of the free energy of polymer chains with respect to the gel volume $P_{in}=-\frac{\partial F}{\partial V}$. Here the total free energy of polymer chains was composed of three parts, i.e. the stretch part because of the stretch of polymer chains during swelling F_{str}, the electrostatic part because of the electrostatic interactions between polymer chain and solvent F_{el}, and the mix part because of the mixing of polymer chains and solvent F_{mix}. These free energy terms were explicitly related to the gel volume, leading to the swelling equilibrium equation

$$\sum_i\left(\frac{\partial F_{str}^i}{\partial V}+\frac{\partial F_{el}^i}{\partial V}+\frac{\partial F_{mix}^i}{\partial V}\right)=P_{ext} \tag{10}$$

where F_{str}^i, F_{el}^i and F_{mix}^i is the three free energy parts of chain i, respectively. Detailed expressions can be found in references [110]. Before solving the swelling equilibrium equation, a specific hydrogel network model is necessary for the summation of the chain force. In order to

obtain a concise expression of total internal force, ideal diamond-lattice network models are adopted to derive the mean-field bulk swelling theories [88, 111], and CG models in diamond lattice are constructed and simulated to verify these swelling theories [88, 93, 111-114]. With these swelling theories, the swelling ratio and the mechanical behavior can be predicted. Unfortunately, few swelling theories from a microscopic view compare their results with experiments, just because of their hydrogel network models differ a lot from real hydrogel network [93, 111].

We provide two ways to investigate the swelling behaviors of PAAm hydrogel. To measure the chemical potential of water in hydrogel is a fundamental way to reveal the swelling mechanism in microscale. The full-atom PAAm hydrogel model [62] was constructed as shown in Fig. 3. By inserting water molecules into PAAm hydrogel model, the chemical potential of water μ_{water} can be obtained by calculating the system energy change

$$\mu_{water} = \frac{\partial W}{\partial N_{water}} \tag{11}$$

where N_{water} is the number of water molecules. Our results demonstrate that the chemical potential of water in PAAm hydrogel gradually increases to that in pure water, when the water content in PAAm hydrogel increases to about 90% during the swelling process. Thus, the water content of about 90% is the swelling limit of PAAm hydrogel. Another indirect way to predict the swelling limit is to obtain the upper limit of water content for forming polymer network. Our investigations [74] on the crosslinking process of PAAm hydrogel show that the water content 97% is the upper limit to form a polymer network. This water content 97% is quite close to the swelling limit of PAAm hydrogels in experiments [52].

Another interesting phenomenon during the swelling-deswelling of hydrogels is the relationship between the elastic modulus and the water content. Experiments found elastic modulus of PAAm hydrogel surges with several orders of magnitude during dehydration. [52, 95, 115, 116] Current constitutive equations [43-45, 48, 117] for hydrogels have given a generic power-law relationship of shear modulus G to the polymer fraction ϕ (or the water content 1- ϕ), i.e., $G \sim \phi^{\frac{1}{3}}$. However, this relationship diverges far from our experimental results which show $E \sim \phi^{0.6}$ in PAAm hydrogels during swelling and $E \sim \phi^{2.3}$ during dehydration [118]. We adopted the SAW network models [118] to explain this abnormal relationship between elastic modulus and water content from a novel perspective. Analogous to the relationship between Young's modulus and elastic wave velocity in solids, we considered that the elastic modulus of the polymer network was proportional to the square of energy transferring velocity through the polymer network $E \sim V^2$. The hydrogel network models were constructed with different water contents as shown in Fig. 9. By simulating the energy transmission process along polymer chains from one lattice point to adjacent lattice points step by step, the energy transferring velocity could be obtained by the passed lattice points divided by the time. Then the relationship between the energy transferring velocity V and the polymer fraction ϕ could be obtained to be $V \sim \phi^{1.16}$ as shown in Fig. 8, leading to $E \sim \phi^{2.32}$. It gives an impressive explanation of the abnormal relationship between elastic constant and water content. However, although this model achieves success to explain the abnormal power-law exponent 2.3 in PAAm hydrogels with lower water content, it fails to explain the exponent 0.6 in PAAm hydrogels with higher water content.

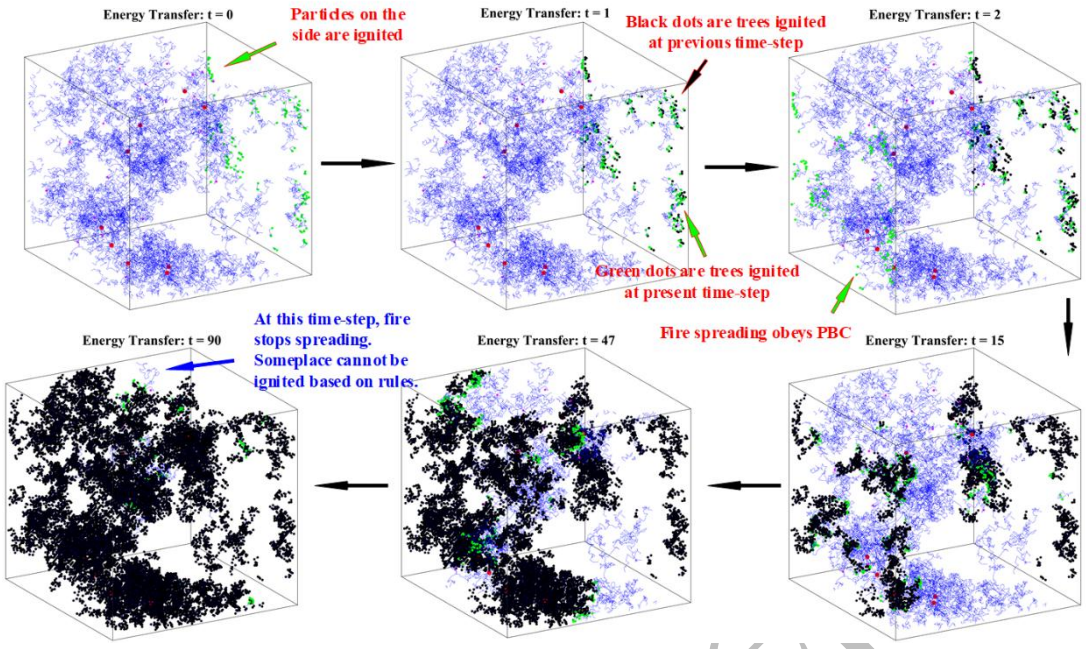

Figure 9 The energy transfer process in hydrogel network model. Reproduced from Ref. [118] with the permission from Li and Liu.

The swelling process of hydrogels includes the stretching of hydrogel network and the interaction between chains and water. Both two parts highly depend on the comprehensive structural properties of hydrogel network. This calls for better hydrogel network models.

3.2 Hyperelasticity

In order to investigate the hyperelastic behavior of hydrogels from a network perspective, the effect of the network randomness is necessary. Alame et al. [108] constructed 2-D STN models with different crosslinker densities and coordination number of crosslinkers. Uniaxial tension simulations were conducted on these STN models. The stress-stretch curves of simulations are compared with constitutive theories using ideal network assumption. It is found that the stress-stretch curves of STN models are quite smooth and agrees well with constitutive

theories based on ideal network assumption. Kothari et al. [109] also constructed similar 2-D STN models to simulate the large deformation and fracture behaviors of hydrogels. The force-stretch curves for independent STN models show almost the same trend until stretched near fracture. We also simulated the large deformation behavior of the PAAm hydrogel models [74]. The nominal stress-stretch curves in Fig. 10 also show the hyperelasticity although the chain lengths in network models are quite random. Above simulation results indicate that the elastic response of hydrogel network is not sensitive to the non-affine deformation of random network models. This is why the constitutive theories based on ideal network assumption describe the hyperelastic response of hydrogels quite well within moderate deformation.

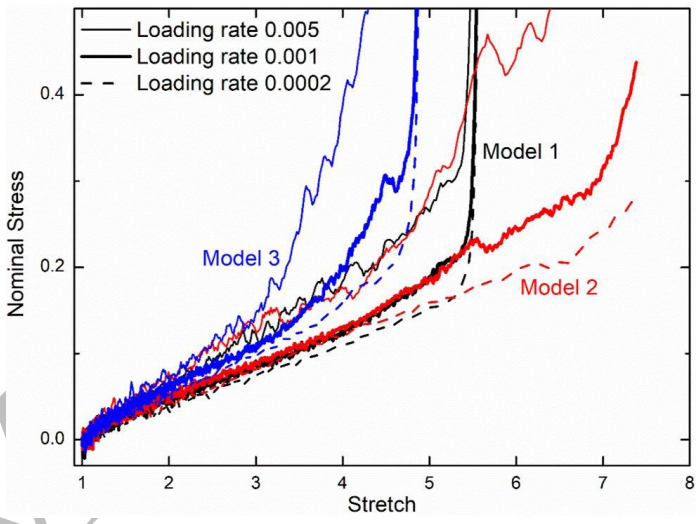

Figure 10 The nominal stress-stretch curves of three independent models in three loading rates. Reproduced from Ref. [74] with the permission from Lei et al.

Above realistic network models and abstract network models do not show advantage to describe the hyperelastic behavior of hydrogels. In order to develop more accurate hydrogel network models for further applications, reproducing the hyperelasticity of hydrogels is always a crucial step for model validation.

3.3 Viscoelasticity

Viscoelasticity is a common mechanical behavior of elastomers. The viscoelasticity experimentally found in hydrogels has two categories, i.e. the loading-history-dependent stress-train behavior and the reversible stress-strain hysteresis. The loading-history-dependent viscoelasticity mainly occurs in multi-network hydrogels. It often shows significant energy dissipation because it mainly caused by the plastic deformation and even chain scission. Many constitutive models [40, 119-121] have been proposed to describe this loading-history-dependent viscoelasticity by assuming the free energy form with respect to both the deformation rate and plastic deformation. However, the fundamental mechanism of viscoelasticity is still ambiguous since current experimental techniques cannot present the network structure. Realistic network models provide intuitive access to the change of chain conformation during viscoelastic deformation. Li et al. [103, 122] constructed CG models of polymer network to measure the structural properties of polymer chains, and used these properties to modify their viscoelastic constitutive equations. However, every chain in their polymer network model was set to have the same monomers, which could no doubt result into exactly the same contour length and quite consistent end-to-end distance. They adopted the equal-chain-length assumption to build network models, and then measured the mean chain length to support the constitutive equations based on the same assumption. This circular argument is a misuse of realistic network models. However, the tube length and the entanglement measured in the polymer network model could be reliable since the randomness of chain conformation is considered. Yin et al. [89] constructed larger CG multi-network models to investigate the viscoelasticity of elastomer network. Figure 11 shows their stress-strain curves of the consecutive loading–unloading cycles. It can be seen that the single network model and double network model are almost pure elastic, while only the triple

network model shows significant load-history-dependent stress-strain hysteresis. This hysteresis agrees quite well with experimental results [123]. Further analysis reveals the energy dissipation in triple network model is caused by irreversible bond breaking which leads to the accumulated damage in each cycle. Loading test along another direction was also simulated on triple network model with pre-exist accumulated damage. It is surprise that the stress-strain curve is not affected by the accumulated damage from another loading direction. Yin et al.'s work [89] indicates that the loading-history-dependent viscoelasticity results from the accumulated damage and shows anisotropy.

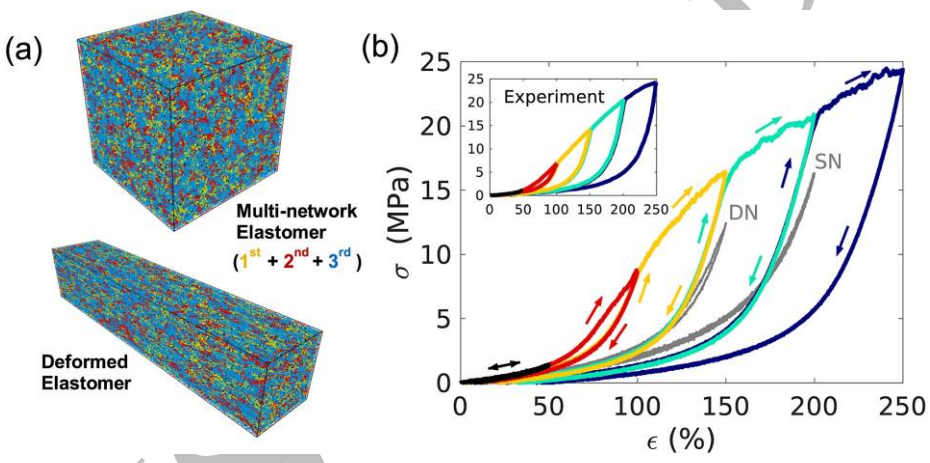

Figure 11 (a) Snapshots of the tripe-network elastomer configuration before and after deformation. (b) Stress–strain curves during loading–unloading cycles with increasing maximum strain. (Inset) Similar stress-strain responses observed in experiments [123]. Reproduced from Ref. [89] with the permission from Elsevier.

The reversible stress-strain hysteresis happens in both single-network hydrogels [51, 115] and double-network hydrogels [54, 124, 125]. Experimental researchers explained that the dissipated energy in this stress-strain hysteresis is caused by the breaking and recovery of sacrificial bonds in hydrogels, such as ionic bonds. However, they cannot explain the stress-

strain hysteresis in single-network neutral hydrogels without sacrificial bonds. We give an interpretation that the stress-strain hysteresis comes from the friction between polymer chains [115]. The friction force acting on a polymer chain relates to the relative slippery velocity with adjacent chains. Since the relative slippery velocity is naturally related to the deformation rate, it connects the friction force with the deformation rate and turns out to be the viscoelastic behavior during macroscopic deformation. This rate-dependent stress-strain hysteresis has been described by many constitutive models [121, 126]. Another finding to support the friction explanation is the increasingly significant viscoelasticity in PAAm hydrogels with decreasing water content. As Fig. 12 shows, water played a role of lubricant in the friction between polymer chains, but the lubrication was always insufficient because the water layer between polymer chains was too thin. Many elaborate experiments have shown that when water is confined in narrow space below nanometer size, its viscosity surges for many orders of magnitude, and it even undergoes a liquid-to-solid transformation. The water layer between polymer chains in hydrogels was calculated to be just confined in such a narrow space. A simple MD model as shown in the insets in Fig. 13 was constructed to validate the lubrication effect of water on the friction force. It simulated the sliding of upper boundary particles and counted the shear force acting on upper boundary particles as shown in Fig. 13. It is clear that the friction force between two boundaries becomes much higher with lower water layer thickness. Since the water layer thickness is directly related to the water content of hydrogels, this qualitative modeling proves that hydrogels with lower water content have more significant viscoelasticity. This reversible viscoelasticity caused by the friction between polymer chains widely exists in all polymeric systems.

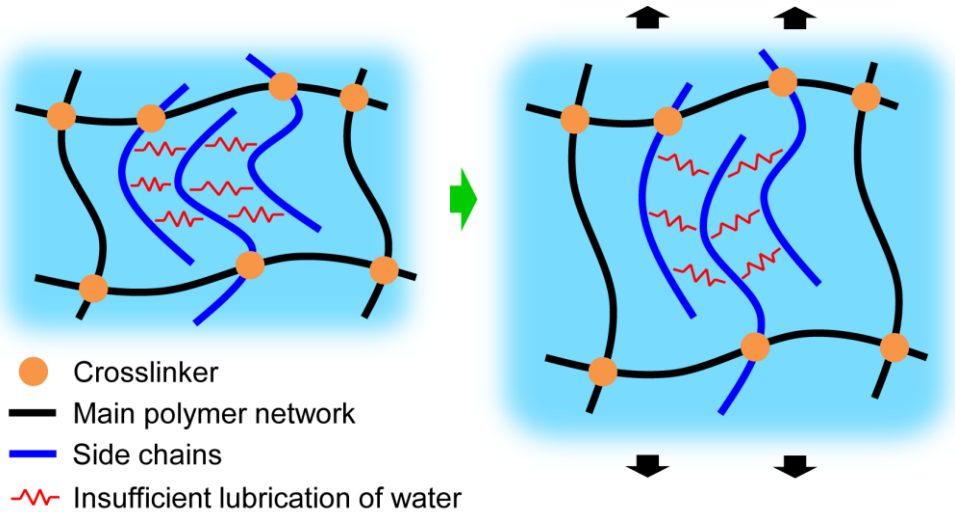

Figure 12 Water plays a role of lubricant for the interaction between polymer chains

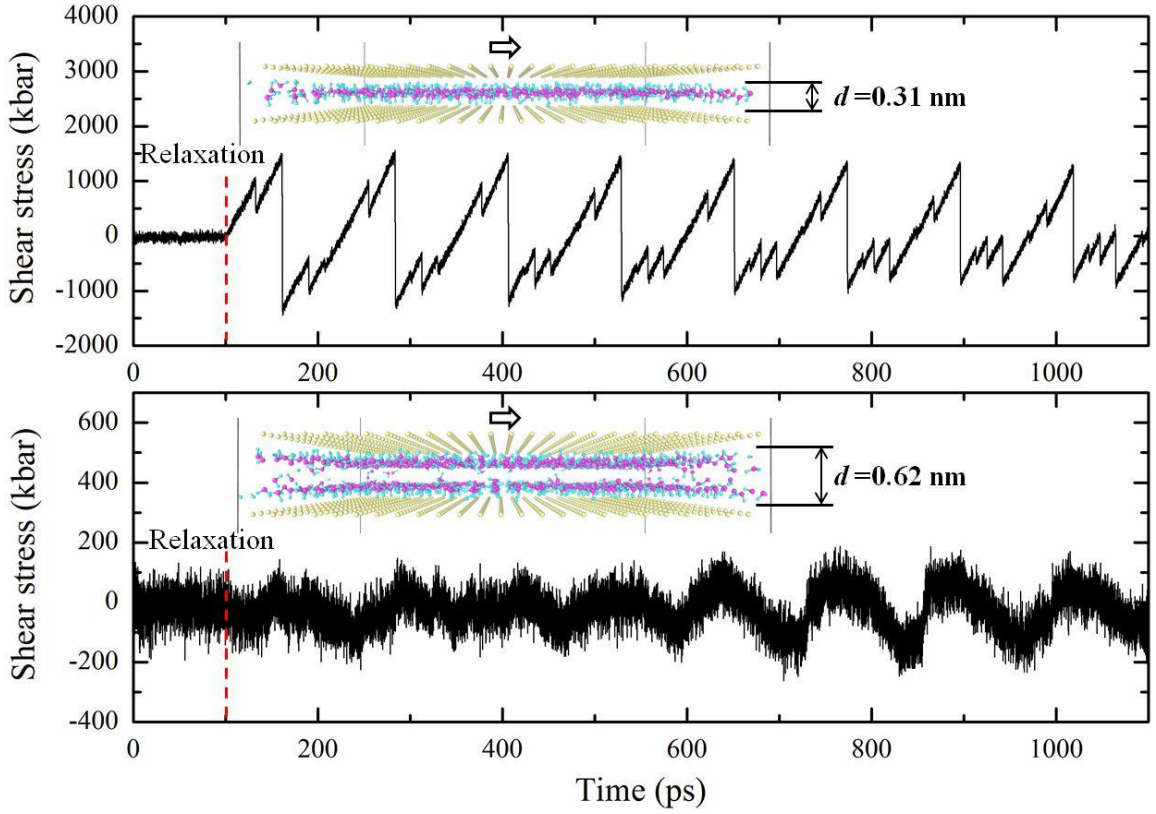

Figure 13 The force-time curves of the sliding simulations. Insets show two CG models. Water layers in two models are confined within different thickness. Yellow particles form the lower and

upper boundaries in two models. Lower boundary is fixed, while upper boundary is sliding. Reproduced from Ref. [115] with the permission from Lei et al.

3.4 Fracture

Compared to the studies on the mechanical behaviors mentioned above, fracture of hydrogels is more suitable to be investigated by network models. It is because the crack initiation and propagation in hydrogels is no longer a bulk behavior which can be statistically summarized into a mean-field theory. Instead, the local structure of the hydrogel network affects the fracture behaviors.

The fracture of a hydrogel network originates from chain scission. For a network model, a fracture criterion for polymer chain is necessary. The simplest fracture criterion is to set a certain ultimate stretch as the fracture criterion for all chains. It is usually adopted in ideal network models to derive the fracture criterion of the entire network. Considering the random chain length distribution in a hydrogel network, every polymer chain may have different fracture stretch. As shown in Fig. 14(a), one reasonable hypothesis is that chain scission occurs when the chain is stretched to straight [61]. Kothari et al. [109] also proposed a fracture criterion for polymer chain with respect to the chain stretch using a transition-state approach. Further, the more fundamental reason for chain scission is that one of the covalent bonds in chain breaks. As shown in Fig. 14(b), two fracture criterions of polymer chain are derived from the stretch criterion of one covalent bond as follows. First, a new free energy form for a single polymer chain is proposed to describe the chain extensibility [50, 57, 74]. This free energy form includes the conformational entropy and the bond stretching energy

$$W = W_{bond}\left(\bar{\lambda}_b\right) + W_{entropy}\left(\frac{\lambda_{chain}}{\bar{\lambda}_b}\right) \tag{12}$$

where $\bar{\lambda}_b$ is the mean bond stretch when a polymer chain is stretched to λ_{chain}, the subscript *b* means bond, $\lambda_{chain}/\bar{\lambda}_b$ is the effective stretch contributing to the conformational entropy. We take the harmonic bond energy and the Langevin-type conformational entropy

$$\begin{aligned} W_{bond} &= \frac{1}{2} N E_b \left(\bar{\lambda}_b - 1\right)^2 \\ W_{entropy} &= nkT\left(\frac{\lambda_{chain}}{\bar{\lambda}_b \lambda_L}\beta + \ln\frac{\beta}{\sinh\beta}\right), \beta = L^{-1}\left(\frac{\lambda_{chain}}{\bar{\lambda}_b \lambda_L}\right) \end{aligned} \tag{13}$$

where E_b is the bond energy coefficient, *N* is the bond number in a chain, *n* is the number of Kuhn segments in a chain, λ_L is the ratio of the contour length to the initial end-to-end distance nb/r_0. Then, it leads to the force balance equation with

$$NE_b\bar{\lambda}_b\left(\bar{\lambda}_b - 1\right) = \frac{nkT}{\lambda_L} L^{-1}\left(\frac{\lambda_{chain}}{\bar{\lambda}_b \lambda_L}\right) \tag{14}$$

This equation gives the relationship between chain stretch to the mean bond stretch. Its physical meaning is that the force acting on this chain results into not only conformational entropy change but also bond stretching. Compared to the restriction of chain stretch $\lambda_{chain} < \lambda_L$ in Langevin free energy form, the new free energy allows an arbitrary chain stretch. The stretch of one individual bond λ_b is not necessary to be the mean bond stretch $\bar{\lambda}_b$ because of the heat fluctuations. Mao et al. [50] neglected the heat fluctuation effect and considered that all bonds were equally stretched during chain deformation, i.e. $\bar{\lambda}_b = \lambda_b$ as shown in Fig. 14(b). They used the stretch criterion of one C-C bond $\lambda_b^f = 1.4$, obtained the fracture criterion of a single polymer chain $\lambda_{chain}^f = 1.41\lambda_L$, which means that fracture occurs when chain is stretched to 1.41 times of the contour length. The

superscript *f* means fracture. However, because of the intrinsic heat fluctuations, this criterion overestimates the chain fracture stretch, which could be an upper limit of chain fracture stretch. Figure 15(a) shows a schematic of the fracture energy of a polymer chain. The energy difference between before and after chain scission is just the energy of one bond. Yet it is not the energy criterion for chain scission. Instead, the energy barrier for chain scission is the energy criterion. We proposed another chain stretch criterion. [74] Since the time scale of the heat fluctuations in polymer chains is far lower than experimental time scale, the energy barrier of the chain scission was totally smoothed out by heat fluctuations. Thus, the fracture energy of a single chain could be just the fracture energy of one bond, leading to the chain stretch criterion

$$\begin{aligned} \lambda_{chain}^{f} &= \bar{\lambda}_b^{f} \lambda_L L\left(\frac{NE_b \bar{\lambda}_b^{f} \lambda_L}{nkT} \left(\bar{\lambda}_b^{f} - 1 \right) \right) \\ \bar{\lambda}_b^{f} &= 1 + \frac{\lambda_b^{f} - 1}{\sqrt{N}} \end{aligned} \tag{15}$$

where λ_b^f is the fracture stretch of one bond, $\bar{\lambda}_b^f$ is the criterion of mean bond stretch in a polymer chain. The fracture stretch of one bond can be obtained by full-atom MD simulations. Figure 15(b) shows the energy-strain curves of the AAm chain with four C-C bonds. Substituting the N=4 and $\bar{\lambda}_b^f = 1.225$ into the second equation in Equation (15), the fracture stretch of one bond is obtained as $\lambda_b^f = 1.45$. Thus the fracture stretch of a polymer chain can also be obtained by the first equation in Equation (15). Our fracture criterion of chain could be a lower limit since the heat fluctuation effect must be overestimated.

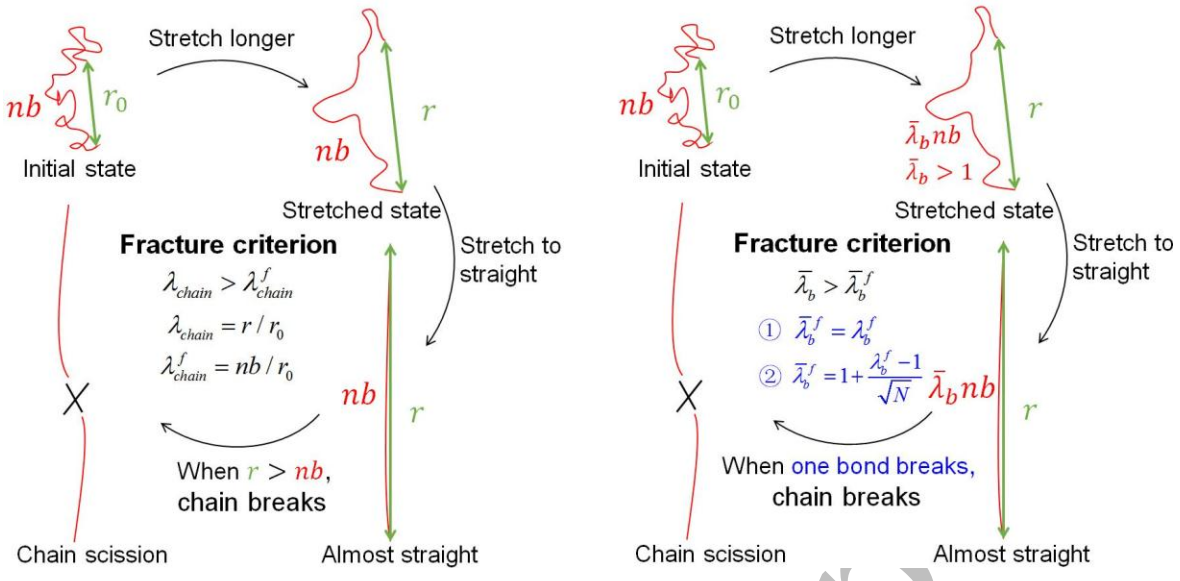

(a) (b)

Figure 14 Schematics of different stretch criterion of a polymer chain. (a) A polymer chain breaks when it is stretched to straight. (b) A polymer chain breaks when one bond in chain breaks. There are two hypotheses to determine the criterion of mean bond stretch $\bar{\lambda}_b^f$. One considers that chain scission occurs when all bonds are stretched to break, leading to the upper limit of chain fracture stretch. Another one considers that the chain fracture energy is equal to the fracture energy of one bond, leading to the lower limit of the chain fracture stretch.

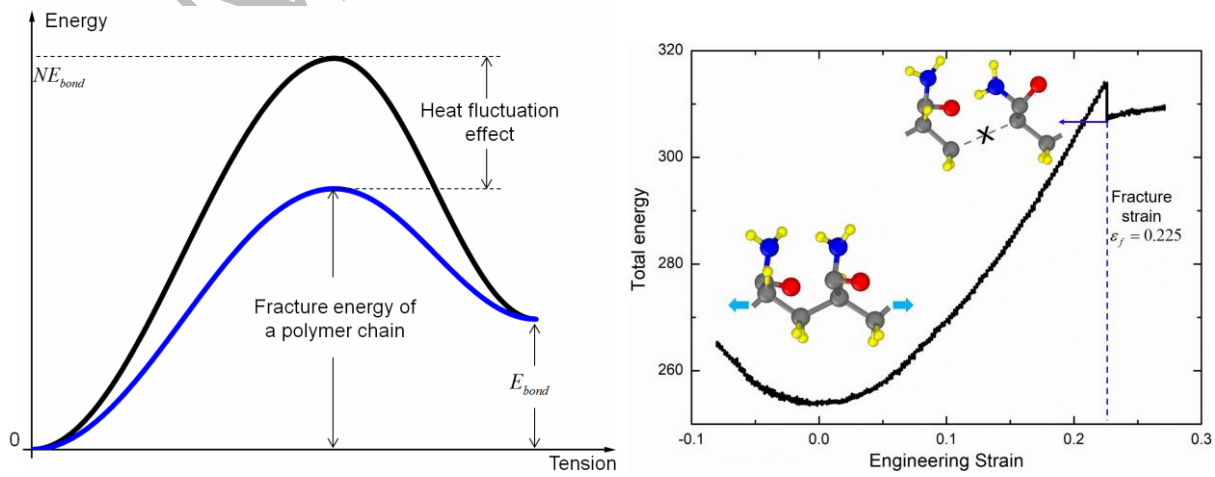

(a) (b)

Figure 15 The fracture energy of a polymer chain. (a) Schematics of the fracture energy of a polymer chain. (b) Fracture energy of one C-C bonds in AAm polymer chain from full-atom MD simulations, reproduced from Ref. [74] with the permission from Lei et al.

Using the fracture criterion shown in Fig. 14(a), we investigate the fracture stretch of hydrogel network model generated by SAW algorithm. [96] SAW network models are converted to logical network as shown in Fig. 16. All chains in hydrogel network are abstracted as a point in logical network. The percolation theory is used to evaluate the connectivity of the logical network. Then, a fraction of rupture chains can be obtained from Fig. 17(a) when the connectivity of logical network reduces to 0, and corresponds to the ultimate stretch 27.79 of hydrogel network as shown in Fig. 17(b).

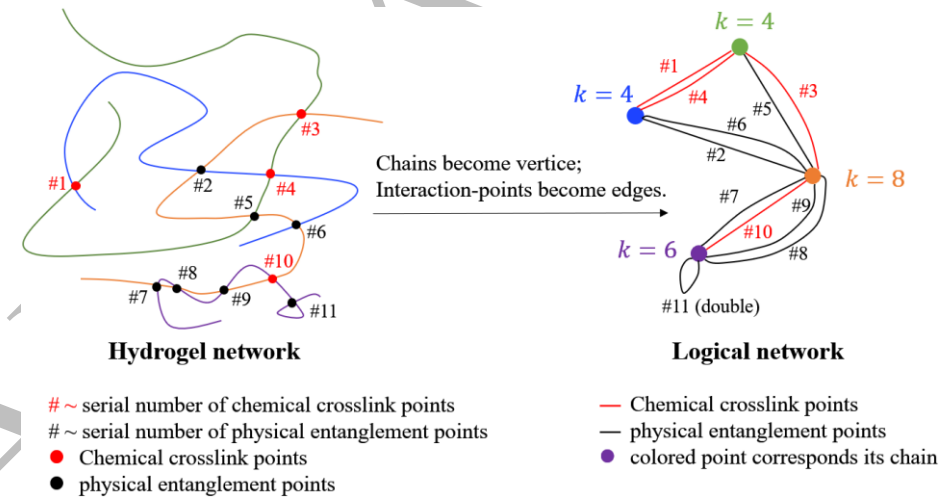

Figure 16 Convert the hydrogel network to a logical network. The left network is the physical network of a hydrogel. The serpentine curves are polymer chains, and there are four chains marked as green, blue, orange, and purple, respectively. Black and red points are interaction points, where black points are physical entanglement points, and red points are

chemical covalent crosslink points, and they are marked with serial numbers. The right-side network is a logical network transformed from the left-side, which shows the interaction relationship of these four polymer chains. Reproduced from Ref. [96] with the permission from Li and Liu.

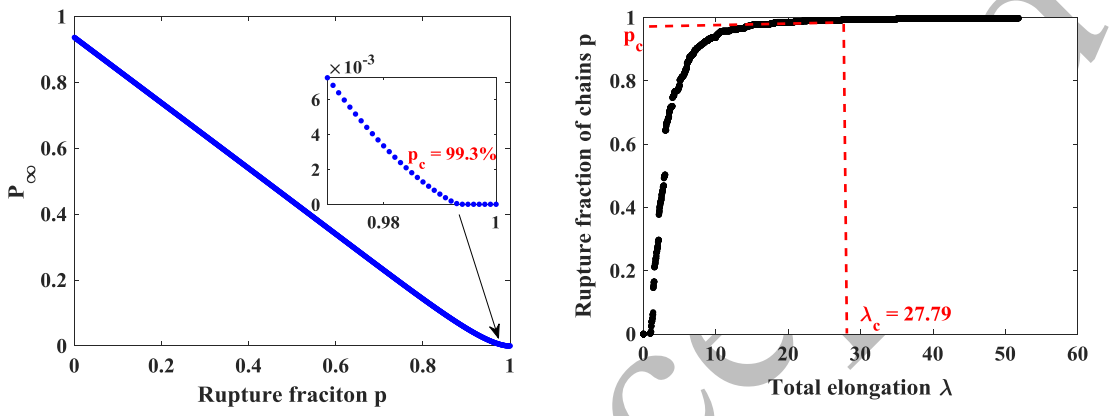

(a) (b)

Figure 17 (a) The relationship between rupture fraction *p* and the connectivity of logical network. (b) The relationship between rupture fraction *p* and the ultimate stretch of hydrogel network model. Reproduced from Ref. [96] with the permission from Li and Liu.

With fracture criterion of a polymer chain, STN models are used to simulate the crack initiation and propagation in hydrogel network. [61, 109] Simulations show that the initial fracture sites (chain scission) are dependent on specific network structure. The following fracture sites tend to develop near the initial fracture sites, and eventually grow to bulk fracture of network. However, the free energy of current STN models always leads to unreal deformation. According to three free energy forms of polymer chain in Equation (3) and (4), the equilibrium length of every polymer chain is 0. Thus, current STN models are actually propped open by

additional boundary conditions, which is of course not physical. More proper free energy of STN models is still in searching.

4. Discussions and Outlook

We have extensively discussed different hydrogel network models and their application to investigate the mechanical properties as shown in Fig. 18. It is necessary to clarify the advantages and disadvantages of these hydrogel network models, and offer a clear orientation to the applications. Full-atom network models provide most detailed atomic structure of polymer network. It is quite useful to investigate the polymer-water interactions, crosslinking mechanism and structural properties of several polymer chains. It is expected to apply full-atom MD to explore functional hydrogels by the modification of monomer (or crosslinker) molecules. However, full-atom network models require huge computational resources, leading to too small model to reflect the statistical properties of hydrogel network. Realistic network models depict the chain conformation with much less atomic details. From realistic network models it is convenient to extract the end-to-end distance distribution, the contour length distribution, mean chain length and chain density. These fundamental structural properties cannot be obtained from experiments. Meanwhile, realistic network models are also suitable to reveal the fundamental mechanism of chain tension/contraction, entanglement and scission, which directly lead to the hyperelasticity, viscoelasticity and fracture of hydrogels. Thus, it is practical to apply realistic network models to design the network structure features, such as branch chains and entanglement, to control the energy dissipation of hydrogels. This can provide guidance on the hydrogel reinforcement and hydrogel adhesion. However, current realistic network models are still too small to capture the bulk mechanical response of hydrogels. STN models focus on the depiction of the random hydrogel network. With much larger model size compared to realistic network

models, it has been applied to investigate the non-affine large deformation of hydrogels with the structural randomness. Furthermore, compared to continuum mechanics and finite element methods, STN models show great advantages on describing fracture of hydrogels because of its intrinsic discontinuity. Fracture behaviors that cannot be observed in experiments, such as the damage accumulation during deformation, the crack initiation and propagation, can be observed from the fracture simulations of STN models. However, current STN models are still too simple to correctly describe the large deformation of hydrogel network. Developing more accurate STN models is a practical way to realize the fracture simulation of hydrogels.

Model	Full-atom Network	Realistic Network	Abstract Network
Governing equation	$\boldsymbol{F}=-\frac{\partial V}{\partial \boldsymbol{x}}, \boldsymbol{F}=m\ddot{\boldsymbol{x}}$	$\boldsymbol{F}^C+\boldsymbol{F}^D+\boldsymbol{F}^R=m\ddot{\boldsymbol{x}}$	$\boldsymbol{F}=-\frac{\partial W}{\partial \boldsymbol{x}}, \boldsymbol{F}+c\dot{\boldsymbol{x}}=m\ddot{\boldsymbol{x}}$
Method	MD [62-69,80,81]	CGMD [70,71,82], DPD [72-74, 83-86,89], user-developed [95,118]	Mean-field theory [50,59,100-103], user-developed [61,108, 109]
Structure	Detailed atomic structure; Siginificant heat fluctuations	Detailed chain conformation; Heat fluctuations	Detailed network structure
Mechanics	Mechanism	Behavior	
	Chain stretch/contract	Swelling [62, 74, 88, 93, 111-114, 118], hyperelasticity [74, 108, 109]	
	Chain interaction	Viscoelasticity [89, 115]	
	Chain scission	Fracture [50, 57, 61, 74, 96, 109]	
Application	Calculate molecular interactions	Analyze real network structrure and interactions	Investigate network topology effect and bulk fracture
Outlook	Design functional hydrogels by monomer (crosslinker) modification	Control energy dissipation in polymer network	Integrate mesoscopic randomness into continuum mechanics

Figure 18 A comprehensive table on the theories, numerical methods, structures, applications and outlook of three types of polymer network models.

Among all these network models, STN models show capability to bridge the microscopic nature and macroscopic mechanical response because of its proper model size. Development of

STN models is still in urgent need in the following directions. First, proper free energy is the basic requirement for further applications of STN models. Introducing the free energy contribution from volumetric deformation may lead to more realistic deformation description of STN models. Second, more precise chain fracture criterion is needed for the bulk fracture description of hydrogels. Statistically considering the heat fluctuation effect may result in accurate chain fracture criterion. Third, STN models are applicable to integrate with finite element methods to develop hybrid simulation methods with both continuous and discrete elements. The numerical implementation of STN model is quite similar to implicit finite element method, since both methods lead to the equation set of $\boldsymbol{K} \cdot \boldsymbol{x} = \boldsymbol{F}$, where $\boldsymbol{K}$ is the stiffness matrix, $\boldsymbol{x}$ is the coordinate vector of all nodes and $\boldsymbol{F}$ is the force vector on all nodes. This similarity makes it possible to unite the simulations of continuous finite elements and discrete STN model, as long as the free energy of two types of models are compatible. At last, the intrinsic non-affine deformation of hydrogels inspires us to rethink the deformation description in continuum mechanics. Besides the widely used deformation gradient, more complete deformation description need to be rigorously established to describe the non-affine deformation in a continuous manner. It is expected to promote the development of continuum mechanics.

5. Conclusions

Advanced applications of hydrogels call for demands to precisely describe the mechanical behaviors, while current constitutive theories face challenges when predicting the extremely large deformation and fracture of hydrogels. Since the hydrogel polymer network dominates the mechanical responses, it is necessary to investigate the fundamental mechanism of these mechanical responses from a network perspective. This work aims to summarize the researches on the theories, structural models and mechanical simulations of hydrogel network,

and provide insights in bridging the gap between microstructure and the macroscopic mechanical behaviors. Hydrogel network possesses complex structures in different length scale, including monomer and crosslinker molecules, Kuhn segments, polymer chains and the random crosslinked network. Hydrogel network models in current researches are divided into three categories, i.e. full-atom network models, realistic network models and abstract network models. Realistic network models can be constructed using full-atom MD, CGMD and DPD methods. The detailed chain conformation makes realistic network models suitable to investigate the swelling-deswelling process, hyperelasticity and viscoelasticity of hydrogels. However, simulating realistic network models with the detailed chain conformation costs too much computational resource, leading to the limited model size. Abstract network models simplify polymer chains into analytical interactions between crosslinking sites. It shows the randomness of the hydrogel network structures and describes the non-affine deformation. Combining with proper fracture criterion of polymer chains, abstract network models show great advantages to simulate the fracture initiation and propagation of hydrogels because of its intrinsic discontinuity. The discrete hydrogel network models are expected to integrate with continuum mechanics to capture the various mechanical behaviors of hydrogels.

Acknowledgement

The authors are grateful for the support from the National Natural Science Foundation of China through grant numbers 11820101001; 11572236; 11372236. The authors are also grateful for the support from the Natural Science Foundation of Shaanxi Province through grant numbers 2020JQ-010. The authors are also grateful for the support from the State Key Laboratory of Nonlinear Mechanics.

References

1. Zheng, Z., Bian, S., Li, Z., et al.: Catechol modified quaternized chitosan enhanced wet adhesive and antibacterial properties of injectable thermo-sensitive hydrogel for wound healing. Carbohydrate Polymers **249**, 116826 (2020) DOI 10.1016/j.carbpol.2020.116826
2. Chen, T., Liu, H., Dong, C., et al.: Synthesis and characterization of temperature/pH dual sensitive hemicellulose-based hydrogels from eucalyptus APMP waste liquor. Carbohydrate Polymers **247**, 116717 (2020) DOI 10.1016/j.carbpol.2020.116717
3. Xian, S., Webber, M.J.: Temperature-responsive supramolecular hydrogels. Journal of Materials Chemistry B **8**, 9197-9211 (2020) DOI 10.1039/d0tb01814g
4. Nourian, A.H., Amiri, A., Moini, N., et al.: Synthesis, test, calibration and modeling of a temperature-actuated hydrogel bilayer. Smart Materials and Structures **29**, 105001 (2020) DOI 10.1088/1361-665X/ab9f46
5. Sun, X.-C., Xia, H., Xu, X.-L., et al.: Ingenious humidity-powered micro-worm with asymmetric biped from single hydrogel. Sensors and Actuators B-Chemical **322**, 128620 (2020) DOI 10.1016/j.snb.2020.128620
6. Zhang, J., Huang, C., Chen, Y., et al.: Polyvinyl alcohol: a high-resolution hydrogel resist for humidity-sensitive micro-/nanostructure. Nanotechnology **31**, 425303 (2020) DOI 10.1088/1361-6528/ab9da7
7. Bian, C., Cheng, Y., Zhu, W., et al.: A Novel Optical Fiber Mach-Zehnder Interferometer Based on the Calcium Alginate Hydrogel Film for Humidity Sensing. Ieee Sensors Journal **20**, 5759-5765 (2020) DOI 10.1109/jsen.2020.2973290
8. Jang, J., Kang, K., Raeis-Hosseini, N., et al.: Self-Powered Humidity Sensor Using Chitosan-Based Plasmonic Metal-Hydrogel-Metal Filters. Advanced Optical Materials **8**, 1901932 (2020) DOI 10.1002/adom.201901932
9. Chen, X., Li, H., Lam, K.Y.: A multiphysics model of photo-sensitive hydrogels in response to light-thermo-pH-salt coupled stimuli for biomedical applications. Bioelectrochemistry **135**, 107584 (2020) DOI 10.1016/j.bioelechem.2020.107584
10. Xing, J., Yang, B., Dang, W., et al.: Preparation of Photo/Electro-Sensitive Hydrogel and Its Adsorption/Desorption Behavior to Acid Fuchsine. Water Air and Soil Pollution **231**, 231 (2020) DOI 10.1007/s11270-020-04582-2
11. Shuai, S., Zhou, S., Liu, Y., et al.: The preparation and property of photo- and thermo-responsive hydrogels with a blending system. Journal of Materials Science **55**, 786-795 (2020) DOI 10.1007/s10853-019-04010-9
12. Li, P., Zhang, J., Dong, C.-M.: Photosensitive poly(o-nitrobenzyloxycarbonyl-L-lysine)-b-PEO polypeptide copolymers: synthesis, multiple self-assembly behaviors, and the photo/pH-thermo-sensitive hydrogels. Polymer Chemistry **8**, 7033-7043 (2017) DOI 10.1039/c7py01574g
13. Shang, J., Theato, P.: Smart composite hydrogel with pH-, ionic strength- and temperature-induced actuation. Soft Matter **14**, 8401-8407 (2018) DOI 10.1039/c8sm01728j

14. Li, W., Jiang, C., Lu, S., et al.: A hydrogel microsphere-based sensor for dual and highly selective detection of Al3+ and Hg2+. Sensors and Actuators B-Chemical **321**, 128490 (2020) DOI 10.1016/j.snb.2020.128490
15. Liao, J., Huang, H.: Smart pH/magnetic sensitive Hericium erinaceus residue carboxymethyl chitin/Fe3O4 nanocomposite hydrogels with adjustable characteristics. Carbohydrate Polymers **246**, 116644 (2020) DOI 10.1016/j.carbpol.2020.116644
16. Ata, S., Rasool, A., Islam, A., et al.: Loading of Cefixime to pH sensitive chitosan based hydrogel and investigation of controlled release kinetics. International Journal of Biological Macromolecules **155**, 1236-1244 (2020) DOI 10.1016/j.ijbiomac.2019.11.091
17. Liu, T.-Y., Hu, S.-H., Liu, K.-H., et al.: Study on controlled drug permeation of magnetic-sensitive ferrogels: Effect of Fe3O4 and PVA. Journal of Controlled Release **126**, 228-236 (2008) DOI 10.1016/j.jconrel.2007.12.006
18. Liu, T.-Y., Hu, S.-H., Liu, T.-Y., et al.: Magnetic-sensitive behavior of intelligent ferrogels for controlled release of drug. Langmuir **22**, 5974-5978 (2006) DOI 10.1021/la060371e
19. Awasthi, S., Gaur, J.K., Bobji, M.S.: Advanced ferrogels with high magnetic response and wear resistance using carbon nanotubes. Journal of Alloys and Compounds **848**, 156259 (2020) DOI 10.1016/j.jallcom.2020.156259
20. Bhattarai, N., Gunn, J., Zhang, M.: Chitosan-based hydrogels for controlled, localized drug delivery. Advanced Drug Delivery Reviews **62**, 83-99 (2010) DOI 10.1016/j.addr.2009.07.019
21. Li, J., Mooney, D.J.: Designing hydrogels for controlled drug delivery. Nature Reviews Materials **1**, 16071 (2016) DOI 10.1038/natrevmats.2016.71
22. Hamedi, H., Moradi, S., Hudson, S.M., et al.: Chitosan based hydrogels and their applications for drug delivery in wound dressings: A review. Carbohydrate Polymers **199**, 445-460 (2018) DOI 10.1016/j.carbpol.2018.06.114
23. Merino, S., Martin, C., Kostarelos, K., et al.: Nanocomposite Hydrogels: 3D Polymer-Nanoparticle Synergies for On-Demand Drug Delivery. Acs Nano **9**, 4686-4697 (2015) DOI 10.1021/acsnano.5b01433
24. Chen, C.H., Tsai, C.C., Chen, W.S., et al.: Novel living cell sheet harvest system composed of thermoreversible methylcellulose hydrogels. Biomacromolecules **7**, 736-743 (2006) DOI 10.1021/bm0506400
25. Cushing, M.C., Anseth, K.S.: Hydrogel cell cultures. Science **316**, 1133-1134 (2007) DOI 10.1126/science.1140171
26. Liebmann, T., Rydholm, S., Akpe, V., et al.: Self-assembling Fmoc dipeptide hydrogel for in situ 3D cell culturing. Bmc Biotechnology **7**, 88 (2007) DOI 10.1186/1472-6750-7-88
27. Shinohara, S., Kihara, T., Sakai, S., et al.: Fabrication of in vitro three-dimensional multilayered blood vessel model using human endothelial and smooth muscle cells and high-strength PEG hydrogel. Journal of Bioscience and Bioengineering **116**, 231-234 (2013) DOI 10.1016/j.jbiosc.2013.02.013
28. Yuk, H., Varela, C.E., Nabzdyk, C.S., et al.: Dry double-sided tape for adhesion of wet tissues and devices. Nature **575**, 169-174 (2019) DOI 10.1038/s41586-019-1710-5
29. Censi, R., Di Martino, P., Vermonden, T., et al.: Hydrogels for protein delivery in tissue engineering. Journal of Controlled Release **161**, 680-692 (2012) DOI 10.1016/j.jconrel.2012.03.002

30. Dimatteo, R., Darling, N.J., Segura, T.: In situ forming injectable hydrogels for drug delivery and wound repair. Advanced Drug Delivery Reviews **127**, 167-184 (2018) DOI 10.1016/j.addr.2018.03.007
31. Wang, R., Li, J., Chen, W., et al.: A Biomimetic Mussel-Inspired epsilon-Poly-L-lysine Hydrogel with Robust Tissue-Anchor and Anti-Infection Capacity. Advanced Functional Materials **27**, 1604894 (2017) DOI 10.1002/adfm.201604894
32. Liu, L., Li, X., Ren, X., et al.: Flexible strain sensors with rapid self-healing by multiple hydrogen bonds. Polymer **202**, 122657 (2020) DOI 10.1016/j.polymer.2020.122657
33. Tian, K., Bae, J., Bakarich, S.E., et al.: 3D Printing of Transparent and Conductive Heterogeneous Hydrogel-Elastomer Systems. Advanced Materials **29**, 1604827 (2017) DOI 10.1002/adma.201604827
34. Huang, Y., Zhong, M., Shi, F., et al.: An Intrinsically Stretchable and Compressible Supercapacitor Containing a Polyacrylamide Hydrogel Electrolyte. Angewandte Chemie-International Edition **56**, 9141-9145 (2017) DOI 10.1002/anie.201705212
35. Lin, S., Yuk, H., Zhang, T., et al.: Stretchable Hydrogel Electronics and Devices. Advanced Materials **28**, 4497-4505 (2016) DOI 10.1002/adma.201504152
36. Zhong, R., Tang, Q., Wang, S., et al.: Self-Assembly of Enzyme-Like Nanofibrous G-Molecular Hydrogel for Printed Flexible Electrochemical Sensors. Advanced Materials **30**, 1706887 (2018) DOI 10.1002/adma.201706887
37. Zhou, Y., Wan, C., Yang, Y., et al.: Highly Stretchable, Elastic, and Ionic Conductive Hydrogel for Artificial Soft Electronics. Advanced Functional Materials **29**, 1806220 (2019) DOI 10.1002/adfm.201806220
38. Liao, M., Wan, P., Wen, J., et al.: Wearable, Healable, and Adhesive Epidermal Sensors Assembled from Mussel-Inspired Conductive Hybrid Hydrogel Framework. Advanced Functional Materials **27**, 1703852 (2017) DOI 10.1002/adfm.201703852
39. Ghorbanoghli, A., Narooei, K.: A new hyper-viscoelastic model for investigating rate dependent mechanical behavior of dual cross link self-healing hydrogel. International Journal of Mechanical Sciences **159**, 278-286 (2019) DOI 10.1016/j.ijmecsci.2019.06.019
40. Lin, J., Zheng, S.Y., Xiao, R., et al.: Constitutive behaviors of tough physical hydrogels with dynamic metal-coordinated bonds. Journal of the Mechanics and Physics of Solids **139**, 103915 (2020) DOI 10.1016/j.jmps.2020.103935
41. Caccavo, D., Cascone, S., Lamberti, G., et al.: Hydrogels: experimental characterization and mathematical modelling of their mechanical and diffusive behaviour. Chemical Society Reviews **47**, 2357-2373 (2018) DOI 10.1039/c7cs00638a
42. Hu, Y., Suo, Z.: VISCOELASTICITY AND POROELASTICITY IN ELASTOMERIC GELS. Acta Mechanica Solida Sinica **25**, 441-458 (2012) DOI 10.1016/s0894-9166(12)60039-1
43. Hong, W., Liu, Z., Suo, Z.: Inhomogeneous swelling of a gel in equilibrium with a solvent and mechanical load. International Journal of Solids and Structures **46**, 3282-3289 (2009) DOI https://doi.org/10.1016/j.ijsolstr.2009.04.022
44. Hong, W., Zhao, X., Zhou, J., et al.: A theory of coupled diffusion and large deformation in polymeric gels. Journal of the Mechanics and Physics of Solids **56**, 1779-1793 (2008) DOI https://doi.org/10.1016/j.jmps.2007.11.010

45. Chester, S.A., Anand, L.: A coupled theory of fluid permeation and large deformations for elastomeric materials. Journal of the Mechanics and Physics of Solids **58**, 1879-1906 (2010) DOI https://doi.org/10.1016/j.jmps.2010.07.020
46. Liu, Y., Zhang, H., Zhang, J., et al.: Constitutive modeling for polymer hydrogels: A new perspective and applications to anisotropic hydrogels in free swelling. European Journal of Mechanics - A/Solids **54**, 171-186 (2015) DOI https://doi.org/10.1016/j.euromechsol.2015.07.001
47. Huang, R., Zheng, S., Liu, Z., et al.: Recent Advances of the Constitutive Models of Smart Materials - Hydrogels and Shape Memory Polymers. International Journal of Applied Mechanics **12**, 2050014 (2020) DOI 10.1142/s1758825120500143
48. Xu, S., Liu, Z.: A nonequilibrium thermodynamics approach to the transient properties of hydrogels. Journal of the Mechanics and Physics of Solids **127**, 94-110 (2019)
49. Chester, S.A., Di Leo, C.V., Anand, L.: A finite element implementation of a coupled diffusion-deformation theory for elastomeric gels. International Journal of Solids and Structures **52**, 1-18 (2015) DOI https://doi.org/10.1016/j.ijsolstr.2014.08.015
50. Mao, Y., Talamini, B., Anand, L.: Rupture of polymers by chain scission. Extreme Mechanics Letters **13**, 17-24 (2017) DOI 10.1016/j.eml.2017.01.003
51. Yang, C., Yin, T., Suo, Z.: Polyacrylamide hydrogels. I. Network imperfection. Journal of the Mechanics and Physics of Solids **131**, 43-55 (2019) DOI https://doi.org/10.1016/j.jmps.2019.06.018
52. Zhang, E., Bai, R., Morelle, X.P., et al.: Fatigue fracture of nearly elastic hydrogels. Soft matter **14**, 3563-3571 (2018) DOI 10.1039/c8sm00460a
53. Zhang, W., Hu, J., Tang, J., et al.: Fracture toughness and fatigue threshold of tough hydrogels. ACS Macro Letters **8**, 17-23 (2018) DOI 10.1021/acsmacrolett.8b00788
54. Bai, R., Yang, Q., Tang, J., et al.: Fatigue fracture of tough hydrogels. Extreme Mechanics Letters **15**, 91-96 (2017) DOI https://doi.org/10.1016/j.eml.2017.07.002
55. Tang, J., Li, J., Vlassak, J.J., et al.: Fatigue fracture of hydrogels. Extreme Mechanics Letters **10**, 24-31 (2017) DOI https://doi.org/10.1016/j.eml.2016.09.010
56. Lavoie, S.R., Millereau, P., Creton, C., et al.: A continuum model for progressive damage in tough multinetwork elastomers. Journal of the Mechanics and Physics of Solids **125**, 523-549 (2019) DOI 10.1016/j.jmps.2019.01.001
57. Li, B., Bouklas, N.: A variational phase-field model for brittle fracture in polydisperse elastomer networks. International Journal of Solids and Structures **182**, 193-204 (2020) DOI 10.1016/j.ijsolstr.2019.08.012
58. Mao, Y., Anand, L.: A theory for fracture of polymeric gels. Journal of the Mechanics and Physics of Solids **115**, 30-53 (2018) DOI 10.1016/j.jmps.2018.02.008
59. Lu, X., Hou, Y., Tie, Y., et al.: Crack nucleation and propagation simulation in brittle two-phase perforated/particulate composites by a phase field model. Acta Mechanica Sinica **36**, 493-512 (2020) DOI 10.1007/s10409-020-00927-6
60. Zheng, S., Liu, Z.: The Machine Learning Embedded Method of Parameters Determination in the Constitutive Models and Potential Applications for Hydrogels. International Journal of Applied Mechanics **13**, 2150001 (2021) DOI 10.1142/s1758825121500010
61. Ghareeb, A., Elbanna, A.: An adaptive quasicontinuum approach for modeling fracture in networked materials: Application to modeling of polymer networks. Journal of the Mechanics and Physics of Solids **137**, 103819 (2020) DOI 10.1016/j.jmps.2019.103819

62. Xu, S., Wang, Y., Hu, J., et al.: Atomic understanding of the swelling and phase transition of polyacrylamide hydrogel. International Journal of Applied Mechanics **8**, 1640002 (2016) DOI 10.1142/S1758825116400020
63. Deshmukh, S., Mooney, D.A., McDermott, T., et al.: Molecular modeling of thermo-responsive hydrogels: observation of lower critical solution temperature. Soft Matter **5**, 1514-1521 (2009) DOI 10.1039/b816443f
64. Sun, T.-Y., Liang, L.-J., Wang, Q., et al.: A molecular dynamics study on pH response of protein adsorbed on peptide-modified polyvinyl alcohol hydrogel. Biomaterials Science **2**, 419-426 (2014) DOI 10.1039/c3bm60213c
65. Ou, X., Han, Q., Dai, H.-H., et al.: Molecular dynamic simulations of the water absorbency of hydrogels. Journal of Molecular Modeling **21**, 231 (2015) DOI 10.1007/s00894-015-2784-0
66. Jiang, X., Wang, C., Han, Q.: Molecular dynamic simulation on the state of water in poly(vinyl alcohol) hydrogel. Computational and Theoretical Chemistry **1102**, 15-21 (2017) DOI 10.1016/j.comptc.2016.12.041
67. Mathesan, S., Rath, A., Ghosh, P.: Molecular mechanisms in deformation of cross-linked hydrogel nanocomposite. Materials Science & Engineering C-Materials for Biological Applications **59**, 157-167 (2016) DOI 10.1016/j.msec.2015.09.087
68. Wang, Y., Li, X., Wei, Q., et al.: Molecular Dynamics Simulation of Mechanical Properties for Poly(vinyl pyrrolidone)/Poly(vinyl alcohol) Hydrogel. Asian Journal of Chemistry **26**, 5378-5382 (2014) DOI 10.14233/ajchem.2014.18116
69. Hou, D., Xu, J., Zhang, Y., et al.: Insights into the molecular structure and reinforcement mechanism of the hydrogel-cement nanocomposite: An experimental and molecular dynamics study. Composites Part B: Engineering **177**, 107421 (2019) DOI 10.1016/j.compositesb.2019.107421
70. Zhang, H., Wang, H., Xu, G., et al.: A molecular dynamics simulation of N-(fluorenyl-9-methoxycarbonyl)-dipeptides supramolecular hydrogel. Colloids and Surfaces a-Physicochemical and Engineering Aspects **417**, 217-223 (2013) DOI 10.1016/j.colsurfa.2012.10.066
71. Salahshoor, H., Rahbar, N.: Multi-scale mechanical and transport properties of a hydrogel. Journal of the Mechanical Behavior of Biomedical Materials **37**, 299-306 (2014) DOI 10.1016/j.jmbbm.2014.05.028
72. Chen, S., Yong, X.: Dissipative particle dynamics modeling of hydrogel swelling by osmotic ensemble method. Journal of Chemical Physics **149**, 094904 (2018) DOI 10.1063/1.5045100
73. Wei, Q., Wang, Y., Zhang, Y., et al.: Aggregation behavior of nano-silica in polyvinyl alcohol/polyacrylamide hydrogels based on dissipative particle dynamics. Polymers **9**, 611 (2017) DOI 10.3390/polym9110611
74. Lei, J., Xu, S., Li, Z., et al.: Study on Large Deformation Behavior of Polyacrylamide Hydrogel Using Dissipative Particle Dynamics. Frontiers in Chemistry **8**, 115 (2020) DOI 10.3389/fchem.2020.00115
75. Kuhn, W., Grün, F.: Beziehungen zwischen elastischen Konstanten und Dehnungsdoppelbrechung hochelastischer Stoffe. Kolloid-Zeitschrift **101**, 248-271 (1942) DOI 10.1007/BF01793684
76. Dauber‐Osguthorpe, P., Roberts, V.A., Osguthorpe, D.J., et al.: Structure and energetics of ligand binding to proteins: Escherichia coli dihydrofolate reductase‐trimethoprim, a

drug‐receptor system. Proteins: Structure, Function, and Bioinformatics **4**, 31-47 (1988) DOI 10.1002/prot.340040106
77. Kaminski, G., Duffy, E.M., Matsui, T., et al.: FREE-ENERGIES OF HYDRATION AND PURE LIQUID PROPERTIES OF HYDROCARBONS FROM THE OPLS ALL-ATOM MODEL. Journal of Physical Chemistry **98**, 13077-13082 (1994) DOI 10.1021/j100100a043
78. Berendsen, H.J.C., Vanderspoel, D., Vandrunen, R.: GROMACS - A MESSAGE-PASSING PARALLEL MOLECULAR-DYNAMICS IMPLEMENTATION. Computer Physics Communications **91**, 43-56 (1995) DOI 10.1016/0010-4655(95)00042-e
79. Mayo, S.L., Olafson, B.D., Goddard, W.A.: DREIDING - A GENERIC FORCE-FIELD FOR MOLECULAR SIMULATIONS. Journal of Physical Chemistry **94**, 8897-8909 (1990) DOI 10.1021/j100389a010
80. Wu, Y., Joseph, S., Aluru, N.R.: Effect of cross-linking on the diffusion of water, ions, and small molecules in hydrogels. The Journal of Physical Chemistry B **113**, 3512-3520 (2009) DOI 10.1021/jp808145x
81. Xu, S., Cai, S., Liu, Z.: Thermal Conductivity of Polyacrylamide Hydrogels at the Nanoscale. ACS Applied Materials & Interfaces **10**, 36352-36360 (2018) DOI 10.1021/acsami.8b09891
82. Marrink, S.J., Risselada, H.J., Yefimov, S., et al.: The MARTINI force field: Coarse grained model for biomolecular simulations. Journal of Physical Chemistry B **111**, 7812-7824 (2007) DOI 10.1021/jp071097f
83. Groot, R.D., Rabone, K.: Mesoscopic simulation of cell membrane damage, morphology change and rupture by nonionic surfactants. Biophysical journal **81**, 725-736 (2001) DOI 10.1016/S0006-3495(01)75737-2
84. Groot, R.D.: Applications of dissipative particle dynamics. Springer, Berlin Heidelberg (2004) DOI 10.1007/978-3-540-39895-0_1
85. Palkar, V., Choudhury, C.K., Kuksenok, O.: Development of Dissipative Particle Dynamics framework for modeling hydrogels with degradable bonds. MRS Advances **5**, 927-934 (2020) DOI 10.1557/adv.2020.148
86. Groot, R.D., Warren, P.B.: Dissipative particle dynamics: Bridging the gap between atomistic and mesoscopic simulation. The Journal of Chemical Physics **107**, 4423-4435 (1997)
87. Longo, G.S., Olvera de la Cruz, M., Szleifer, I.: Molecular Theory of Weak Polyelectrolyte Gels: The Role of pH and Salt Concentration. Macromolecules **44**, 147-158 (2011) DOI 10.1021/ma102312y
88. Landsgesell, J., Sean, D., Kreissl, P., et al.: Modeling Gel Swelling Equilibrium in the Mean Field: From Explicit to Poisson-Boltzmann Models. Physical Review Letters **122**, 208002 (2019) DOI 10.1103/PhysRevLett.122.208002
89. Yin, Y., Bertin, N., Wang, Y., et al.: Topological origin of strain induced damage of multi-network elastomers by bond breaking. Extreme Mechanics Letters **40**, 100883 (2020) DOI 10.1016/j.eml.2020.100883
90. Zidek, J., Milchev, A., Vilgis, T.A.: Dynamic behavior of acrylic acid clusters as quasi-mobile nodes in a model of hydrogel network. The Journal of Chemical Physics **137**, 244908 (2012) DOI 10.1063/1.4769833

91. Zidek, J., Jancar, J., Milchev, A., et al.: Mechanical Response of Hybrid Cross-Linked Networks to Uniaxial Deformation: A Molecular Dynamics Model. Macromolecules **47**, 8795-8807 (2014) DOI 10.1021/ma501504z
92. Zidek, J., Milchev, A., Jancar, J., et al.: Deformation-induced damage and recovery in model hydrogels - A molecular dynamics simulation. Journal of the Mechanics and Physics of Solids **94**, 372-387 (2016) DOI 10.1016/j.jmps.2016.05.013
93. Košovan, P., Richter, T., Holm, C.: Modeling of Polyelectrolyte Gels in Equilibrium with Salt Solutions. Macromolecules **48**, 7698-7708 (2015) DOI 10.1021/acs.macromol.5b01428
94. Mann, B.A.F., Kremer, K., Lenz, O., et al.: Hydrogels in Poor Solvents: A Molecular Dynamics Study. Macromolecular Theory and Simulations **20**, 721-734 (2011) DOI 10.1002/mats.201100050
95. Li, Z., Liu, Z.: Energy transfer speed of polymer network and its scaling-law of elastic modulus-New insights. Journal of Applied Physics **126**, 215101 (2019) DOI 10.1063/1.5129621
96. Li, Z., Liu, Z.: The elongation-criterion for fracture toughness of hydrogels based on percolation model. Journal of Applied Physics **127**, 215101 (2020) DOI 10.1063/5.0009626
97. Wall, F.T.: Statistical thermodynamics of rubber. III. Journal of Chemical Physics **11**, 527-530 (1943) DOI 10.1063/1.1723793
98. Grest, G.S., Kremer, K.: MOLECULAR-DYNAMICS SIMULATION FOR POLYMERS IN THE PRESENCE OF A HEAT BATH. Physical Review A **33**, 3628-3631 (1986) DOI 10.1103/PhysRevA.33.3628
99. Doi, M.Edwards, S.F., *Theory of polymer dynamics*. Theory of polymer dynamics. 1986.
100. Davidson, J.D., Goulbourne, N.C.: A nonaffine network model for elastomers undergoing finite deformations. Journal of the Mechanics and Physics of Solids **61**, 1784-1797 (2013) DOI https://doi.org/10.1016/j.jmps.2013.03.009
101. Xiang, Y., Zhong, D., Wang, P., et al.: A general constitutive model of soft elastomers. Journal of the Mechanics and Physics of Solids **117**, 110-122 (2018) DOI 10.1016/j.jmps.2018.04.016
102. Arruda, E.M., Boyce, M.C.: A three-dimensional constitutive model for the large stretch behavior of rubber elastic materials. Journal of the Mechanics and Physics of Solids **41**, 389-412 (1993) DOI https://doi.org/10.1016/0022-5096(93)90013-6
103. Ying, L., Tang, S., Kröger, M., et al.: Molecular simulation guided constitutive modeling on finite strain viscoelasticity of elastomers. Journal of the Mechanics and Physics of Solids **88**, 204-226 (2016) DOI https://doi.org/10.1016/j.jmps.2015.12.007
104. Davidson, J.D., Goulbourne, N.C.: Nonaffine chain and primitive path deformation in crosslinked polymers. Modelling and Simulation in Materials Science and Engineering **24**, 065002 (2016) DOI 10.1088/0965-0393/24/6/065002
105. Zhang, L., Feng, X., Li, S.: Review and perspective on soft matter modeling in cellular mechanobiology: cell contact, adhesion, mechanosensing, and motility. Acta Mechanica **228**, 4095-4122 (2017) DOI 10.1007/s00707-017-2057-3
106. Broedersz, C.P., MacKintosh, F.C.: Modeling semiflexible polymer networks. Reviews of Modern Physics **86**, 995-1036 (2014) DOI 10.1103/RevModPhys.86.995

107. Colombo, J., Widmer-Cooper, A., Del Gado, E.: Microscopic Picture of Cooperative Processes in Restructuring Gel Networks. Physical Review Letters **110**, 198301 (2013) DOI 10.1103/PhysRevLett.110.198301
108. Alame, G., Brassart, L.: Relative contributions of chain density and topology to the elasticity of two-dimensional polymer networks. Soft Matter **15**, 5703-5713 (2019) DOI 10.1039/c9sm00796b
109. Kothari, K., Hu, Y., Gupta, S., et al.: Mechanical Response of Two-Dimensional Polymer Networks: Role of Topology, Rate Dependence, and Damage Accumulation. Journal of Applied Mechanics-Transactions of the Asme **85**, 031008 (2018) DOI 10.1115/1.4038883
110. Katchalsky, A., Michaeli, I.: POLYELECTROLYTE GELS IN SALT SOLUTIONS. Journal of Polymer Science **15**, 69-86 (1955) DOI 10.1002/pol.1955.120157906
111. Landsgesell, J., Holm, C.: Cell Model Approaches for Predicting the Swelling and Mechanical Properties of Polyelectrolyte Gels. Macromolecules **52**, 9341-9353 (2019) DOI 10.1021/acs.macromol.9b01216
112. Schneider, S., Linse, P.: Swelling of cross-linked polyelectrolyte gels. European Physical Journal E **8**, 457-460 (2002) DOI 10.1140/epje/i2002-10043-y
113. Mann, B.A., Kremer, K., Holm, C.: The swelling behavior of charged hydrogels. Macromolecular Symposia **237**, 90-107 (2006) DOI 10.1002/masy.200650511
114. Lu, Z.Y., Hentschke, R.: Computer simulation study on the swelling of a polyelectrolyte gel by a Stockmayer solvent. Physical Review E **67**, 061807 (2003) DOI 10.1103/PhysRevE.67.061807
115. Lei, J., Zhou, Z., Liu, Z.: Side Chains and the Insufficient Lubrication of Water in Polyacrylamide Hydrogel—A New Insight. Polymers **11**, 1845 (2019)
116. Lv, H.B., Leng, J.S., Liu, Y.J., et al.: Shape-memory polymer in response to solution. Advanced Engineering Materials **10**, 592-595 (2008) DOI 10.1002/adem.200800002
117. Xu, S., Liu, Z.: Coupled theory for transient responses of conductive hydrogels with multi-stimuli. Journal of the Mechanics and Physics of Solids **143**, 104055 (2020) DOI https://doi.org/10.1016/j.jmps.2020.104055
118. Li, Z., Liu, Z., Ng, T.Y., et al.: The effect of water content on the elastic modulus and fracture energy of hydrogel. Extreme Mechanics Letters **35**, 100617 (2020) DOI 10.1016/j.eml.2019.100617
119. Diani, J., Brieu, M.Gilormini, P.: Observation and modeling of the anisotropic visco-hyperelastic behavior of a rubberlike material. International Journal of Solids and Structures **43**, 3044-3056 (2006) DOI 10.1016/j.ijsolstr.2005.06.045
120. Drozdov, A.D., Sanporean, C.G., Christiansen, J.d.C.: Mechanical response of HEMA gel under cyclic deformation: Viscoplasticity and swelling-induced recovery. International Journal of Solids and Structures **52**, 220-234 (2015) DOI 10.1016/j.ijsolstr.2014.10.009
121. Mao, Y., Lin, S., Zhao, X., et al.: A large deformation viscoelastic model for double-network hydrogels. Journal of the Mechanics and Physics of Solids **100**, 103-130 (2017) DOI https://doi.org/10.1016/j.jmps.2016.12.011
122. Li, Y., Tang, S., Abberton, B.C., et al.: A predictive multiscale computational framework for viscoelastic properties of linear polymers. Polymer **53**, 5935-5952 (2012) DOI https://doi.org/10.1016/j.polymer.2012.09.055

123. Ducrot, E., Chen, Y., Bulters, M., et al.: Toughening Elastomers with Sacrificial Bonds and Watching Them Break. Science **344**, 186-189 (2014) DOI 10.1126/science.1248494
124. Bai, R., Yang, J., Morelle, X.P., et al.: Fatigue Fracture of Self-Recovery Hydrogels. ACS Macro Letters **7**, 312-317 (2018) DOI 10.1021/acsmacrolett.8b00045
125. Webber, R.E., Creton, C., Brown, H.R., et al.: Large Strain Hysteresis and Mullins Effect of Tough Double-Network Hydrogels. Macromolecules **40**, 2919-2927 (2007) DOI 10.1021/ma062924y
126. Parada, G.A., Zhao, X.: Ideal reversible polymer networks. Soft Matter **14**, 5186-5196 (2018) DOI 10.1039/c8sm00646f